Renewable and Sustainable Energy Reviews 72 (2017) 1104–1123

Contents lists available at ScienceDirect

Renewable and Sustainable Energy Reviews

journal homepage: www.elsevier.com/locate/rser

Assessment of photovoltaic performance models for system simulation

Justo José Roberts[a,*], Andrés A. Mendiburu Zevallos[b], Agnelo Marotta Cassula[a]

[a] UNESP, Univ Estadual Paulista, Department of Electrical Engineering, Campus of Guaratinguetá, Av. Ariberto Pereira da Cunha, 333, Guaratinguetá, SP 12510410, Brazil

[b] UNESP, Univ Estadual Paulista, Energy Department, Campus of Guaratinguetá, Av. Ariberto Pereira da Cunha, 333, Guaratinguetá, SP 12510410, Brazil

ARTICLE INFO

Keywords:
Experimental data
Mathematical model
Performance
Photovoltaic energy
Renewable energy
Uncertainty

ABSTRACT

An essential stage in assessing the feasibility of a PV project is the energy yield prediction, which estimates the total energy production of a PV system at a specific site. Photovoltaic (PV) performance models are mathematical representations used to estimate the energy yield of power systems based on PV technology. The PV performance models are subjected to a series of errors derived from the different steps in the modeling chain of the PV system. Although some studies have been conducted to assess the accuracy of these models, limited research have focused on studying the accuracy of the individual submodels that comprise the PV performance model. The main objective of this paper is to assess the performance of different combinations of the most cited models aiming to find a PV performance model with good accuracy. There were studied a total of 20 PV performance models derived from the combination of four plane-of-the-array (POA) irradiance models, five PV module models and two inverter models. All the PV performance models were implemented computationally and their performance was compared with measurements collected by a data acquisition system in a real 2.2 kWp photovoltaic system. The best PV performance model presents an accuracy of −0.201% (rMBE) and 15.099% (rRMSE) with respect to the measured AC power output, which is in line with the values reported in the literature. Several sources of error were identified, which can greatly influence PV system energy yield estimation. Among them, the uncertainty in the derating factors which represent all the non-temperature dependent losses present in the PV system is the most critical.

1. Introduction

Brazil is an emerging economy which has been growing rapidly in the last decade, both economically and demographically. As a consequence, the rising living standard of the population makes the supply of secure and sustainable energy one of the most important aspects for the economy. The Brazilian Minister of Mines and Energy projected a 90% increase in electric energy consumption until 2030 compared to the current consumption levels [1]. In order to face this problem, the Brazilian government is seeking to develop all sectors of power generation. Currently, the energy generation relies mainly on hydroelectricity, which accounted for nearly 70% of the total electricity generation in 2014 [1]. However, due to recent droughts that reduced dramatically the electricity generation and lead the energy sector into crisis, the Brazilian government has shifted its focus towards diversifying its energy mix to include other renewable energy sources. Among them, solar energy is one of the most promising, since the country is located in a region where solar radiation is one of the highest in the world [2].

In order to diversify and decentralize the energy sector, the Brazilian government introduced in 2012 the net-metering mechanism. This feed-in law allows business and residential consumers to feed into the grid the electricity they produced with renewables, and earn credits in their electricity bill [3]. With this new regulation scenario, solar photovoltaic (PV) generation is expected to be more profitable, thus encouraging the PV energy production in the residential and commercial sectors. Given the right regulation scenario that guarantees the feed in of all energy produced, the main uncertainty for an investment in a PV project is the expected energy production. Thus, right from the beginning of any PV project a study of the expected energy yield is essential to assess the financial risk of the investment. An energy yield prediction is an estimate of the total energy production of a PV system at a specific site [4]. The energy yield prediction is done with PV performance models.

Photovoltaic performance models are mathematical representations used to estimate the energy generation of power systems based on PV technology. These models predict the energy generation of the PV system based on specifications of the system (PV modules, inverters,

* Corresponding author.
E-mail address: justo@feg.unesp.br (J.J. Roberts).

http://dx.doi.org/10.1016/j.rser.2016.10.022
Received 1 March 2016; Received in revised form 27 August 2016; Accepted 16 October 2016
Available online 28 October 2016
1364-0321/

installation characteristic, etc.) and meteorological data (solar irradiance, ambient temperature, wind speed, etc.). PV performance models range from simplified models, which are based on general assumptions regarding system components and loss factors, to more complex models that consider information provided by manufacturers, estimated parameters and empirical relationships to reach closer to reality results [5].

Photovoltaic system modeling and simulation is subjected to a series of errors that need to be identified and quantified in order to manage the financial risk of an investment in PV system. These errors derive from the different steps in the modeling chain of the PV system [6]. In order to understand what confidence can be placed to the PV performance models for energy yield prediction, it is necessary to quantify the errors introduced in each step of the model. Confidence in PV performance models helps projects secure competitive financing and more accurately characterize expected performance.

To date, limited amount of research studies have been conducted to assess the accuracy of PV performance models. The bulk of them are limited to compare the accuracy of commercially available PV performance tools [7–9] and some of them lack a comparison with measurement data from real PV systems. Not much work has studied the individual submodels' accuracy [10] in order to identify a configuration that minimizes the aggregated error of the PV performance model as a whole.

An article presented in 2008 by Cameron et al. [10] compares the performance of a simulation tool developed by the U.S. Energy Department, the System Advisor Model (SAM), with actual measurements of a PV system performance. The authors conclude that SAM is able to predict the PV energy generation with great accuracy, but improvements related to the system derating factors and the radiation models should be further studied. The authors Klise and Stein [11] presented a comprehensive report that documents various PV performance models and simulation software developed and utilized by researchers at Sandia National Laboratories. This report is limited to present the main characteristics of the models and does not perform any comparison of their accuracy. An article published in 2010 by Yates and Hibberd [7] presents a theoretical review of the main aspects to be considered when developing a PV performance model, highlighting the sources of error derived from the simplifications considered by the models. In the same work, five commercial simulation software (PVWatts, SAM, PVsyst, PVSol and PV-DesignPro) are tested and compared with real data derived from two systems in operation in the United States. Similarly, Lee, Frearson and Rodden [8] presented a study in which four commercial simulation software (PVsyst, HOMER, RETScreen and SMA Sunny Design) are evaluated and their performances compared with data collected in six PV systems of different technologies located in the Australian dessert. The authors found that there are a large number of uncertainties that influence the energy yield of the performance models analyzed, but an experienced user with quality input data can minimize the error with respect to actual yield. More recently, Freeman et al. [9] presented a study were they validated five commercially available performance modeling tools with quality-controlled measured performance data. The authors concluded that the more detailed performance modeling tools examined present an annual error (predicted - measured) within 8% when using the default values of derating factors.

In order to obtain a realistic view of the behavior of a PV system, it is necessary to achieve computer simulations. But it is inevitable that the models would present inaccuracies derived by the assumptions made when representing a real system with mathematical equations. To be aware of the magnitude of these inaccuracies, there is a need to study the available PV performance models in order to identify and quantify the sources of error these models contain.

The objective of the present article is to assess the performance of different combinations of the most cited models aiming to conform a PV performance model with good accuracy that can be used to predict the energy yield of PV projects. To do so, 16 combinations of decomposition-transposition models were implemented in order to select four best POA irradiance models. These four POA irradiance models were then coupled with five PV module models and two inverter model resulting in a total of 20 PV system performance models. All these models were computationally implemented in Matlab® and their performances compared with measured data collected in a photovoltaic installation of 2.2 kWp. The best PV performance model presented an accuracy of −0.201% (rMBE) and 15.099% (rRMSE) with respect to the measured AC power output.

2. PV performance models

At the most simplest level, the PV performance models come down to two main stages: (i) estimate how much solar irradiance reaches the PV array; and (ii) estimate the electricity generated by the PV system from the incoming solar irradiance. In the first stage, models to estimate the solar irradiance incident on the plane-of-the-array (POA) must be employed, whereas for the second stage, mathematical models that estimate the power generated by the PV modules given the POA irradiance are implemented. Other secondary stages include the power conditioning systems that take the power output of the PV array and transform it to the desired form, depending on the characteristics of the load to be served. In Fig. 1 it is depicted the layout of the modeling process for a PV system with AC output. In the following sections, it is presented the theoretical concepts of the POA irradiance models and the PV module models implemented in the present work, as well as the considerations adopted with respect to the remaining components of the system.

2.1. Plane of the array irradiance models

Typical meteorological data includes values of global solar irradiance incident on a horizontal plane (GHI), which indicates the total amount of solar radiation reaching the horizontal surface of the earth. However, the power output of the PV array depends on the POA irradiance, which is the amount of radiation reaching the surface of the array, inclined with respect to the horizontal in order to maximize incident solar radiation along the year [12]. Estimating the POA irradiance from the GHI involves two steps [13]: (i) the decomposition of the GHI into its direct and diffuse components, generally expressed as diffuse horizontal irradiance (DHI) and direct normal irradiance (DNI), also known as beam irradiance; and (ii) the transposition of these components to the plane-of-the-array. For each of these two step, various models have been proposed in the literature [14], but no combination of decomposition and transition models is widely accepted as standard for converting GHI to POA irradiance [13,15]. In the following section, the specific models implemented in the present work are presented.

2.1.1. Decomposition models

The decomposition models considered in the present study are

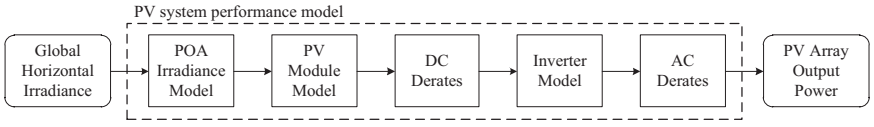

Fig. 1. PV system modeling layout.

Table 1
Decomposition models implemented.

Model	Type	Input variables	Abbreviation
Orgill and Hollands[16]	Piecewise empirical	GHI, k_t	OH
Erbs et al.[18]	Piecewise empirical	GHI, k_t	Er
Maxwell[19]	Quase-physical	GHI, k_t, θ_{el}, p	DISC
Ineichen et al.[20]	Quase-physical	GHI, k_t, θ_{el}, p, T_a	DIRINT

presented in Table 1. While this is not an exhaustive list of all the available models, it includes some of the most cited decomposition models. They can be classify as piecewise empirical models, which are purely empirical models based on correlations between the clearness index ($k_t = GHI/E_a$) and the diffuse fraction ($k_d = DHI/GHI$), where E_a is extraterrestrial irradiance. And quasi-physical models, which are developed using physical principles and also incorporate empirical relationships. Most of the decomposition models estimate the diffuse fraction, which is then converter into DHI by multiplying by the GHI. Other models, compute the direct fraction and hence the DNI, derived from Eq. (1):

$$DNI = \frac{GHI - DHI}{\sin(\theta_{el})} \tag{1}$$

where θ_{el} is the solar elevation angle.

2.1.1.1. Orgill and Hollands model (OH). The Orgill and Hollands [16] decomposition model is one of the first models that implemented the approach of linking DHI and GHI through empirical correlations as proposed by [17]. The authors [16] developed this model based on data collected in Toronto, Canada, resulting in Eq. (2).

$$k_d = \begin{cases} 1 - 0.24k_t & for\ \ k_t \le 0.35 \\ 1.577 - 184k_t & for\ \ 0.35 < k_t \le 0.75 \\ 0.177 & for\ \ k_t > 0.75 \end{cases} \tag{2}$$

2.1.1.2. Erbs et al. model (Er). The authors Erbs et al. [18] implemented the same approach as Orgill and Hollands [16] based on collected data at five stations in the USA at latitudes between 31° and 42°N. The correlation proposed by Erbs et al. [18] is shown in Eq. (3).

$$k_d = \begin{cases} 1 - 0.09k_t & for\ \ k_t \le 0.22 \\ 0.9511 - 0.1604k_t + 4.388k_t^2 - 16.638k_t^3 + 12.336k_t^4 & for\ \ 0.22 < k_t \le 0.80 \\ 0.165 & for\ \ k_t > 0.8 \end{cases} \tag{3}$$

2.1.1.3. Maxwell model (DISC). Maxwell [19] proposed a quasi-physical model for converting hourly GHI to DNI. The model combines physical principles with experimental correlation functions for various conditions. The original computer program that implemented Maxwell's model was called Direct Insolation Simulation Code, thus the model is also known as DISC [19]. The model initiates by calculating a clear-sky direct beam transmittance (Kn_c) as a function of the air mass (AM).

$$Kn_c = 0.866 - 0.122(\mathrm{AM}) + 0.0121(AM)^2 - 0.000653(AM)^3 + 0.000014(\mathrm{AM})^4 \tag{4}$$

Then, a reduction of Kn_c is computed with Eq. (5).

$$Kn = Kn_c(\mathrm{AM}) - \Delta Kn(AM, k_t) \tag{5}$$

where ΔKn is computed using the Eq. (6).

$$\Delta Kn = a(k_t) + b(k_t)\exp[c(k_t)\cdot \mathrm{AM}] \tag{6}$$

The air mass is computed from Eq. (7)

$$\mathrm{AM} = [\cos(\theta_z) + 0.15(93.885 - \theta_z)^{-1.253}]^{-1} \cdot \frac{p}{1013.25} \tag{7}$$

where θ_z is the sun's zenith angle and p is the local air pressure. The coefficients a, b and c, function of the clearness index, are derived from the Eqs. (8) and (9).

$$\begin{cases} a = -5.74 + 21.77k_t - 27.49k_t^2 + 11.56k_t^3 \\ b = 41.40 - 118.50k_t + 66.05k_t^2 + 31.09k_t^3 \quad for\ \ k_t > 0.6 \\ c = -47.01 + 184.2k_t - 222.0k_t^2 + 73.81k_t^3 \end{cases} \tag{8}$$

$$\begin{cases} a = 0.512 - 1.56k_t + 2.286k_t^2 - 2.222k_t^3 \\ b = 0.370 - 0.962k_t \quad for\ \ k_t \le 0.6 \\ c = -0.280 + 0.932k_t - 2.048k_t^2 \end{cases} \tag{9}$$

Finally, the DNI is computed using Eq. (10).

$$DNI = E_a \cdot K_n \tag{10}$$

2.1.1.4. Ineichen et al. model (DIRINT). Ineichen et al. [20] developed a model for determining DNI from GHI as an improvement to the DISC model. This model [20], also known as DIRINT model, improves the estimation by binning zenith angle, global horizontal transmittance, and dew point temperature; or various functions of these variables, including a time derivative of the global horizontal transmittance. Each parameterization or "bin" is indicative of the sky condition. The impact of each possible bin is given by finding a coefficient from a four-dimensional look-up table, and using this coefficient to modify the estimated DNI result from the DISC model.

2.1.2. Transposition models

The next step consists in estimating the POA irradiance based on the sum of the incident beam, diffuse and ground reflectance solar irradiance components:

$$POA = POA_{beam} + POA_{diff} + POA_{refl} \tag{11}$$

Several transposition models have been proposed in the literature [17,21–41]. In general, all of them estimate the beam irradiance incident in the plane-of-the-array (POA_{beam}) in the same way [7]; from the DNI through the geometric expression (12).

$$POA_{beam} = DNI \cdot \cos(\mathrm{AOI}) \tag{12}$$

where AOI is the angle of incidence between the sun's rays and the PV array, obtained from Eq. (13).

$$\mathrm{AOI} = \cos^{-1}[\cos(\theta_z)\cos(\beta) + \sin(\theta_z)\sin(\beta)\cos(\theta_A - \theta_{A,array})] \tag{13}$$

where θ_A is the solar azimuth; β and $\theta_{A,array}$ are the tilt and azimuth angles of the array, respectively.

The reflected fraction of the solar irradiance (POA_{refl}) is computed as a function of the GHI, the reflectivity of the ground surface or albedo (ρ_g), and the tilt angle of the surface, under the hypothesis of isotropic reflection and constant albedo in the field of view [42].

$$POA_{refl} = GHI \cdot \rho_g \left(\frac{1 - \cos\beta}{2}\right) \tag{14}$$

Where the models differ is in the treatment of the diffuse irradiance (POA_{diff}), according to the approach adopted, they can be broadly classify as isotropic sky models and anisotropic sky models [43]. The former ones assume that the intensity of diffuse sky irradiance is

Table 2
Transposition models implemented.

Model	Type	Input variables	Abbreviation
Liu and Jordan [22]	Isotropic sky	β, DHI	LJ
Koronakis [23]	Isotropic sky	β, DHI	Ko
HDKR [28]	Anisotropic sky	β, $\theta_{A,array}$, DHI, DNI, GHI, E_a, θ_A, θ_z	HDKR
Perez et al. [35]	Anisotropic sky	β, $\theta_{A,array}$, DHI, DNI, E_a, θ_A, θ_z,AM	Pe

uniform over the sky dome, thus with this assumption the diffuse irradiance is the same regardless of the orientation and depends on the fraction of the sky dome seen by the surface [44]. The anisotropic models assume the anisotropy of the diffuse sky irradiance at the horizon and in the circumsolar region [7,43].

Table 2 present the transposition models studied in the present work. There were implemented the two most cited isotropic sky models, Liu and Jordan [22] and Koronakis [23], and two anisotropic sky models, the HDKR [28] and the Perez et al. [35].

2.1.2.1. Liu and Jordan isotropic sky model (LJ). This model was first proposed by Hottel and Woertz [45] and then an improvement was made by Liu and Jordan [22], as cited in [28]. The total solar irradiance on a tilt surface is supposed to include three components: beam, isotropic diffuse and reflected from the ground. The circumsolar diffuse and the horizon diffuse radiation fluxes are neglected. The beam and ground reflected irradiance components are estimated using Eqs. (12) and (14), respectively, the diffuse component ($POA_{LJ,diff}$) is computed with Eq. (15).

$$POA_{LJ,diff} = DHI\left(\frac{1 + \cos\beta}{2}\right) \tag{15}$$

2.1.2.2. Koronakis isotropic sky model (Ko). Koronakis [23] proposed a modification to the Liu and Jordan [22] model based on the assumption that the southern part of the sky is responsible for 63% of diffuse solar flux. The modified equation is (16):

$$POA_{Ko,diff} = DHI\left(\frac{2 + \cos\beta}{3}\right) \tag{16}$$

2.1.2.3. Hay, Davies, Klucher and Reindl anisotropic sky model (HDKR). The authors Duffie and Beckman [28] proposed the combination of three models proposed by Hay and Davies [34], Klucher [33] and Reindl et al. [27] to account for the three diffuse irradiance components (isotropic diffuse, circumsolar diffuse and horizon diffuse). This model, named HDKR, is not much complex than the isotropic model and gives better estimations of irradiance on tilted surfaces. According to the HDKR model, the beam and ground reflected irradiance components are computed with Eqs. (12) and (14), and the diffuse component ($POA_{HDKR,diff}$) is as calculated with Eq. (17):

$$POA_{HDKR,diff} = DHI\left\{A_i\cos(AOI) + (1 - A_i)\left(\frac{1 + \cos\beta}{2}\right)\left[1 + f\sin^3\left(\frac{\beta}{2}\right)\right]\right\} \tag{17}$$

where $A_i = DNI/E_a$ is the anisotropy index calculated as the ratio of the the beam irradiance and the the extraterrestrial radiation (E_a); and $f = \sqrt{DNI\cdot\cos(\theta_z)/GHI}$ is a modulation factor that takes into account the horizon brightening.

2.1.2.4. Perez et al. anisotropic sky model (Pe). Perez et al. [35] presented a new model where the isotropic, circumsolar and horizon diffuse radiation are analyzed in a more detailed manner. This model differs from the isotropic and HDKR models in that it uses empirical coefficients derived from measurements over a range of sky conditions and locations instead of mathematical representations of the sky diffuse components [46,47]. According to this model, the diffuse solar irradiance incident on a tilted surface is given by Eq. (18):

$$POA_{Pe,diff} = DHI\left[(1 - F_1)\left(\frac{1 + \cos\beta}{2}\right) + F_1\frac{a}{b} + F_2\sin\beta\right] \tag{18}$$

where F_1 and F_2 are empirical functions of the sky clearness and describe circumsolar and horizon brightness, respectively. The coefficients a and b are terms that account for the angle of incidence of the sun onto the inclined surface, calculated as $a = \max(0, \cos(\text{AOI}))$ and $b = \max(\cos(85°), \cos(\theta_z))$.

The brightness coefficients (F_1 and F_2) are derived from the so called Perez coefficients that describe the sky conditions, the zenith angle, the clearness, and the brightness. In the present work, the Perez coefficients taken from [35] are used.

In the Perez et al. model the beam and ground reflected irradiance components are also computed with Eqs. (12) and (14) [35].

2.2. PV module models

The second main stage in the modeling of PV systems is to determine the energy output of the solar cell, module or array. Several PV module models have been proposed, both simple models with few input parameters to more complex models with more extensive PV module characterization procedures [11]. They can be classify into two categories, power models and models based on the equivalent electric circuit of the PV cell [48]. In the present work, two models from the first class are studied, the model implemented by the software HOMER [49] and the model proposed by Diaf et al. [50], based on the simplified model from Evans [51]. Also three other models from the second group are studied, the models proposed by De Soto et al. [52], Villalva et al. [53,54], and Walker [55].

2.2.1. Power models

The power models [56–58] are based on a single point efficiency representation of the PV module. They estimate the power delivered by the PV module when operating at Maximum Power Point (MPP), and depending on the complexity of the model it can estimate the power output under varying operational conditions with acceptable precision. Following the power models implemented in the present work.

2.2.1.1. HOMER model. The hybrid power system optimization software HOMER [49] uses this model to estimate the PV array power output. In Eq. (19) the power delivered by the PV array is proportional to the solar irradiance incident upon the plane of the array, POA [W/m^2], independent of the temperature and the voltage to which is exposed, see first two terms in Eq. (19). To model the effect of temperature on the efficiency of the PV array, a third term is introduced which depends on the difference between the actual PV cell temperature, T_c [ºC], and the cell temperature at Standard Test Conditions (STC), $T_{c,STC}$ [ºC], and on the temperature coefficient of power, α_p [%/ºC]. A fourth term, called PV derating factor, f_{pv} [%], is a power reduction factor that considers all the non-temperature

dependent looses. Finally, the inverter's losses are considered through an efficiency factor, η_{inv}[%]. In Eq. (19) Y_{pv} [kW] is the rated capacity of the PV array and POA_{STC} is the incident irradiance at STC (1 kW/m^2).

$$P_{pv} = Y_{pv}\left(\frac{POA}{POA_{STC}}\right)\underbrace{[1+\alpha_p(T_c - T_{c,STC})]}_{temperature\ \ effect} f_{pv}\,\eta_{inv} \tag{19}$$

The temperature of the cell under operating conditions is estimated from the explicit Eq. (20) derived from the energy balance for a unit module area proposed by [28]. It is considered that the PV array always works at its maximum power point (the system is supposed to have a maximum power point tracker), and that the cell efficiency is equal to maximum power point efficiency at STC ($\eta_c = \eta_{mp,STC}$). With the above assumptions, the cell temperature under any operating condition of solar radiation and ambient temperature is:

$$T_c = \frac{T_a + (T_{c,NOCT} - T_{a,NOCT})\left(\frac{POA}{POA_{NOCT}}\right)\left[1 - \frac{\eta_{mp,STC}(1-\alpha_p T_{c,NOCT})}{\tau\alpha}\right]}{1 + (T_{c,NOCT} - T_{a,NOCT})\left(\frac{POA}{POA_{NOCT}}\right)[\frac{\alpha_p \eta_{mp,STC}}{\tau\alpha}]} \tag{20}$$

where T_a is the ambient temperature [ºC]; $T_{c,NOCT}$ is the cell temperature at Nominal Operating Cell Temperature (NOCT) [ºC]; $T_{a,NOCT}$ is the ambient temperature at which the NOCT is defined [20 °C]; POA_{NOCT} is the incident irradiance at which the NOCT is defined [0.8 kW/m^2]; and $\tau\alpha$ is the effective transmittance-absorptance product of the PV module (considered equal to 0.9 according to [28]).

2.2.1.2. Diaf et al. model. Evans [51] proposed a simplified model to estimate the electrical output of photovoltaic arrays; it combines basic characteristic parameters of the PV array (datasheet information) with meteorological information to determine the efficiency of the PV array. This model is implemented by Diaf et al. [50] with some modifications.

The power output of the PV generator is calculated according to Eq. (21).

$$P_{pv} = (\eta_{pv} N_{pv} A_{pv}) POA \cdot f_{pv} \tag{21}$$

where η_{pv} is the instantaneous PV generator efficiency, N_{pv} is the number of PV panels, A_{pv} [m^2] is the area of the PV array and f_{pv} [%] is a power reduction factor.

The instantaneous PV generator efficiency is represented by Eq. (22).

$$\eta_{pv} = \eta_{mp,STC}\eta_{mpt}[1 - \alpha_p(T_c - T_{c,STC})] \tag{22}$$

where η_{mpt} is the efficiency of the MPP tracking system, and $T_{c,STC}$ is the cell temperature at Standard Test Conditions [ºC].

Based on the energy balance proposed by [28] and assuming that the overall heat loss can be estimated from the nominal operating cell temperature [59], the PV cell temperature is approximated by Eq. (23).

$$T_c = T_a + POA\left(\frac{T_{c,NOCT} - 20}{800}\right) \tag{23}$$

By substituting Eq. (23) into (22), the instantaneous PV generator efficiency can be expressed as follows.

$$\eta_{pv} = \eta_{mpp,STC}\eta_{mpt}\left[1 - \alpha_p(T_a - T_{c,STC}) - \alpha_p POA\left(\frac{T_{c,NOCT} - 20}{800}\right)\right] \tag{24}$$

where $\eta_{mp,STC}$, α_p, $T_{c,NOCT}$ and A_{pv} are parameters that depend on the PV cell technology and are generally provided by the manufacturer through the module's datasheet.

2.2.2. Models based on the equivalent electric circuit

The power models are only able to estimate the power output of the PV array when working at its maximum power point. But, when it is necessary to know the full current vs voltage (I–V) characteristic curve of the the PV cell, models for calculating the electrical characteristics of the PV cell under varying operating conditions are needed [60]. Different approaches have been proposed to approximate the I-V curve, ranging from empirical models [61] to interpolation techniques to approximate the I-V curve [62]. But among all the most used approach is to represent the PV cell by an equivalente electric circuit. That is, the operation of a solar cell can be represented by an electrical equivalent circuit composed of a current source, one or two parallel diodes and combinations of series and parallel resistances. Depending on the type of device, the required accuracy and/or availability of information, different mathematical models may be adopted [63]. The double-diode model, initially proposed by Wolf and Rauschenbach [64], is especially accurate when dealing with low illumination conditions, but not interesting when simulating solar modules under real operating conditions when the PV system will operate mostly at high levels of solar radiation [65]. The review to the literature reveals that the one-diode circuit model is the more commonly used in engineering applications, since it offers a good compromise between simplicity and accuracy [53,66]. Therefore, this type of PV cell model is adopted in the present work.

The one-diode equivalent circuit is shown in Fig. 2(a) and the corresponding characteristic equation is Eq. (25). In this case, five parameters need to be determined to completely characterize the equation: the light current (I_L); the diode saturation current (I_o); the series resistance (R_s); the shunt resistance (R_{sh}) and the diode ideality factor (n). $V_t = N_c T_c k/q$ is the module thermal voltage with N_c cells connected in series, T_c [K] is the cell temperature, k is the Boltzmann's constant (1.381×10^{-23} J/K) and q is the electron charge (1.605×10^{-19} C).

$$I = I_L - I_D - I_{sh} = I_L - I_o\left[\exp\left(\frac{V + IR_s}{nV_t}\right) - 1\right] - \frac{V + IR_s}{R_{sh}} \tag{25}$$

In practice, the shunt resistance presents a high value, thus some authors consider it infinite and therefore neglect it [55,67–69]. This simplification leads to the second version of the one-diode equivalent circuit shown in Fig. 2(b) and its characteristic Eq. (26), were only four parameter need to be determined.

$$I = I_L - I_D - I_{sh} = I_L - I_o\left[\exp\left(\frac{V + IR_s}{nV_t}\right) - 1\right] \tag{26}$$

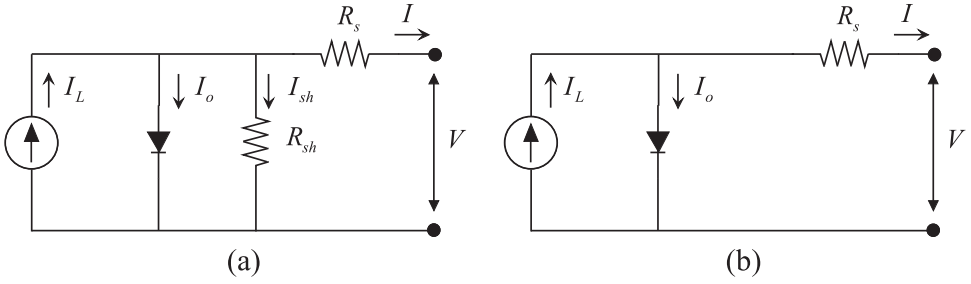

Fig. 2. Equivalent electric circuit of the one-diode PV cell representation: (a) considering shunt and series resistances; (b) considering the shunt resistance infinite.

In order to use the electric circuit models, the parameters of the characteristic equation (I_L,I_o, R_s, R_{sh} and n) which are different for each type of PV module, need to be determined. This is a nontrivial endeavor due the simultaneous equations are usually non-linear and include exponential terms. Several parameter extraction methods have been proposed in recent years; these methods can be classified into three categories such as analytic, iterative and evolutionary computational methods [66]. Analytic methods [65,70,71] introduce a series of simplifications and approximations that lead to rapid calculation. Nevertheless, their accuracy at non-standard operating conditions is proved to be poor [72]. Iterative methods [52,53,63] employ numerical methods to solve the non-linear equations associated with the PV model. Numerical methods are widely employed since they provide a reasonable compromise between simplicity, accuracy and speed of calculation. On the other hand, these methods largely depend on the initial conditions, which affects its accuracy and convergence [72]. In recent years, artificial intelligence algorithms have been utilized for the parameter extraction of the PV models [60,73–78]. Despite of reaching to more accurate results, artificial intelligence techniques require extensive simulation times as reported in [60].

In the present work, it is aimed a low complexity model, with relative good accuracy, easy to be implemented computationally and that uses only information provided by the PV module manufacturer. Hence, from the literature review performed it can be concluded that the one-diode equivalent circuit combined with an iterative method to extract the parameters of the characteristic equation is the best choice. The equivalent-circuit-based models implemented here are explained following.

2.2.2.1. De Soto, Klein and Beckman model. The methodology proposed by De Soto et al. [52] is based on the one-diode, one series resistance and one shunt resistance model presented in Fig. 2(a). The characteristic equation is (25) with the only difference that the authors [52] consider a different factor called modified ideality factor defined as:

$$a = \frac{nkT_cN_s}{q} \tag{27}$$

In this model the five parameters (unknowns) that need be determined are I_L, I_o, R_s, R_{sh} and a, thus at least five equations are needed for solving the problem. De Soto et al. [52] propose to use the reference values provided by the manufacturer at STC to evaluate the five unknown parameters. All the parameters with "*ref*" sub index are at reference conditions (STC), while the others are at specified operating conditions.

a) The short-circuit condition, when $V = 0$ and $I = I_{sc,ref}$

$$I_{sc,ref} = I_{L,ref} - I_{o,ref}\left[\exp\left(\frac{I_{sc,ref}R_{s,ref}}{a_{ref}}\right) - 1\right] - \frac{I_{sc,ref}R_{s,ref}}{R_{sh,ref}} \tag{28}$$

b) The open-circuit condition, when $V = V_{oc,ref}$ and $I = 0$

$$I_{sc,ref} = I_{L,ref} - I_{o,ref}\left[\exp\left(\frac{V_{oc,ref}}{a_{ref}}\right) - 1\right] - \frac{V_{oc,ref}}{R_{sh,ref}} \tag{29}$$

c) The maximum power point condition, when $I = I_{mp,ref}$ and $V = V_{mp,ref}$

$$I_{mp,ref} = I_{L,ref} - I_{o,ref}\left[\exp\left(\frac{V_{mp,ref} + I_{mp,ref}R_{s,ref}}{a_{ref}}\right) - 1\right] - \frac{V_{\mathrm{mp},ref} + I_{mp,ref}R_{s,ref}}{R_{sh,ref}} \tag{30}$$

d) The fourth condition is the assumption that the derivative of the power with respect to voltage is zero at maximum power point, leading to the next equation

$$\left.\frac{\partial P}{\partial V}\right|_{P=P_{mp}} = 0 \rightarrow \quad \frac{I_{mp,ref}}{V_{mp,ref}} = \frac{\frac{I_{o,ref}}{a_{ref}}\exp\left(\frac{V_{mp,ref}+I_{mp,ref}}{a_{ref}}\right) + \frac{1}{R_{sh,ref}}}{1 + \frac{I_{o,ref}R_{s,ref}}{a_{ref}}\exp\left(\frac{V_{mp,ref}+I_{mp,ref}R_{s,ref}}{a_{ref}}\right) + \frac{R_{s,ref}}{R_{sh,ref}}} \tag{31}$$

e) And the final condition ensures the model is in accordance with the temperature coefficient of open-circuit ($\mu_{V,oc}$)

$$\mu_{V,oc} = \frac{\partial V_{oc}}{\partial T} \approx \frac{V_{oc}(T_c) - V_{oc}(T_{c,ref})}{T_c - T_{c,ref}} \tag{32}$$

where T_c is the cell temperature.

To determine $\mu_{V,oc}$ it is necessary to know the open-circuit voltage at a cell temperature different from the reference temperature, $V_{oc}(T_c)$. To this extent the temperature dependence of I_L, I_o a, R_{sh} and R_s are necessary.

The light depends directly on the effective incident solar radiation (S), on the cell temperature and on the short-circuit temperature coefficient $\mu_{I,sc}$:

$$I_L = \frac{S}{S_{ref}}[I_{L,ref} + \mu_{I,sc}(T_c - T_{c,ref})] \tag{33}$$

The variation of the reverse saturation current with the operating temperature is explained with the next equation:

$$\frac{I_o}{I_{o,ref}} = \left(\frac{T_c}{T_{c,ref}}\right)^3 \exp\left[\frac{E_g}{kT}\Big|_{T_{c,ref}} - \frac{E_g}{kT}\Big|_{T_c}\right]$$
$$\frac{E_g}{E_{g,ref}} = 1 - C(T - T_{c,ref}) \tag{34}$$

where E_g is the material band gap energy. $E_{g,ref}$=1.12 eV (1.794×10^{-19} J) and C =0.0002677 for silicon.

The modified ideality factor is assumed to linearly depend on the cell temperature:

$$\frac{a}{a_{ref}} = \frac{T_c}{T_{c,ref}} \tag{35}$$

According to the authors [52], the shunt resistance is inversely proportional to the short-circuit current; therefore, to the solar radiation:

$$\frac{R_{sh}}{R_{sh,ref}} = \frac{S_{ref}}{S} \tag{36}$$

With respect to the series resistance, it is assumed independent both on temperature and radiation:

$$R_s(T_{c,ref}\ ,\ S_{ref}) = R_s(T_c\ ,\ S) \tag{37}$$

The information needed to determine the parameters at reference conditions is completed. The four Eqs. (28)–(31) relate the model to the known reference parameters. And to evaluate (32) the temperature dependence Eqs. (33)–(37) are used, leading to the fifth relation that completes the system of equations.

$$\frac{S}{S_{ref}}[I_{L,ref} + \mu_{I,sc}(T_c - T_{c,ref})] =$$
$$I_o\left[\exp\left(\frac{\mu_{V,oc}(T_c - T_{c,ref}) + V_{oc}(T_{c,ref})}{a}\right) - 1\right] + \frac{\mu_{V,oc}(T_c - T_{c,ref}) + V_{oc}(T_{c,ref})}{R_{sh}(T_c)} \tag{38}$$

Now the model is complete, there are five Eqs. (28)–(31) and (38) and five unknowns, the parameters at reference conditions $I_{L,ref}$,$I_{o,ref}$,$R_{s,ref}$,$R_{sh,ref}$ and a_{ref}. All the equations must be solved simultaneously; the authors De Soto et al. [52] used the Engineering Equation Solver (EES) to do so, however the method used for solving the system of equations is not known. In this work it is used the Trust

Region dog-leg method [79] implemented in the optimization toolbox of Matlab [80] for that purpose. The initial guess values needed for the algorithm are the ones proposed by Duffie and Beckman [28].

Once the 5 parameters are known at reference conditions, one can find the parameters at any operating conditions (different levels of solar radiation and temperature) using Eqs. (33)–(37). To determine the PV module output current, I, for a given value of V, Eq. (25) must be numerically solved as $g(V, I) = I - f(V, I) = 0$.

To calculate the array's DC power output it is assume that all of the modules in the array operate uniformly at the same maximum power point (MPP). Although the MPP tracker is not explicitly modeled, it is assumed the system has this equipment. Therefore, by multiplying a single module's DC output, it is obtained the array's DC power output, Eq. (39). Finally, the net AC array's power output is obtained by reducing the array's DC power output with the system losses and the inverter's efficiency, as in Eq. (40):

$$P_{pv,dc} = A_{pv} N_s N_p \; POA \; \eta_{mp} \tag{39}$$

$$P_{pv,ac} = A_{pv} N_s N_p \; POA \; \eta_{mp} f_{pv} \; \eta_{inv} \tag{40}$$

Where N_s is the number of PV modules per string (in series), N_p is the number of strings in parallel and $\eta_{mp} = I_{mp} V_{mp} / I_T A_{pv}$ is the MPP efficiency at new operating conditions. All the non-temperature dependent losses present in the system are included in the global derating factor, f_{pv}, and in the inverter's efficiency η_{inv}. Here the inverter's efficiency is computed with the model presented in Section 2.3.

In this model, the cell temperature at any operating condition is estimated as follows:

$$T_c = T_a + (T_{c,NOCT} - T_{a,NOCT}) \left(\frac{POA}{POA_{NOCT}} \right) \frac{9.5}{5.7 + 3.8 V_w} \left[1 - \frac{\eta_{mp}}{\tau\alpha} \right] \tag{41}$$

where V_w [m/s] is the wind speed. In Eq. (41), the PV operating cell temperature is given in implicit form, i.e. it involves variables which themselves depend on T_c, such as η_{mp}. Thus, to estimate the cell temperature an iteration procedure was implemented [81].

2.2.2.2. Villalva, Gazoli and Ruppert Filho model. The Villalva et al. [53,54] methodology is based on the one-diode, one series resistance and one shunt resistance model presented in Fig. 2(a) and the corresponding characteristic Eq. (25). The approach presented by authors [53,54] consists basically in finding the parameters of the I–V characteristic Eq. (25) by adjusting the curve at three remarkable points: open-circuit, maximum power and short circuit, derived by the manufacturer. The method includes the effect of the series and parallel resistances, and warranties that the maximum power of the model matches with the maximum power of the real PV module.

The assumptions made by Villalva et al. [53] to determine the parameters are:

a) In the original algorithm proposed by Villalva et al. [53], the diode ideality factor n is arbitrarily chosen within the range $n \in [1, 1.5]$, though the accuracy may be improved by running more iterations for different values of n.
b) A new equation for the diode saturation current (I_o) is proposed, which includes the open-circuit voltage coefficient ($\mu_{V,oc}$), and the short-circuit current temperature coefficients ($\mu_{I,sc}$):

$$I_o = \frac{I_{sc,ref} + \mu_{I,sc}(T_c - T_{c,ref})}{\exp\left(\frac{V_{oc,ref} + \mu_{V,oc}(T_c - T_{c,ref})}{\frac{nkT_cN_s}{q}} \right) - 1} \tag{42}$$

c) The relationship between the series resistance and the shunt resistance is considered equal to:

$$I_{L,ref} = \frac{R_{sh} + R_s}{R_{sh}} I_{sc,ref} \tag{43}$$

d) Finally, the same assumption used in [52] with respected to the light current (I_L) is made. It depends linearly on the solar radiation and on the temperature according to the Eq. (33).

With the above considerations, the only remain unknowns in Eq. (25) are R_s and R_{sh}. To determine these resistances, Villalva et al. [53] propose adjusting its values based on the fact that there is only a pair $\{R_s, R_{sh}\}$ that warranties that the calculated maximum power point is equal to the experimental maximum power point provided in the module's datasheet.

An iterative process is proposed, were R_s is gradually incremented starting from $R_s \approx 0$ and adjusting the P–V curve to match the experimental data for various values of $\{R_s, R_{sh}\}$. The initial value of R_{sh} is given by:

$$R_{sh,\,\min} = \frac{V_{mp}}{I_{sc,ref} - I_{mp}} - \frac{V_{oc,ref} - V_{mp}}{I_{mp}} \tag{44}$$

The values of the series and shunt resistances are initially unknown, but as the solution of the algorithm is refined along successive iterations, the values of R_s and R_{sh} converge toward the best solution. For every value of R_s, Eq. (25) must be numerically solved as $g(V, I) = I - f(V, I) = 0$ for a set of V values and obtaining the correspondent I points. In the present work this is done by means of Newton-Rapshon's method.

Finally, the net AC power delivered by the PV array, assuming equipped with a MPP tracker, can be determined by Eq. (40), estimating the inverter's efficiency with the model presented in Section 2.3. The Villalva et al. [53] model assumes that the cell temperature is known, hence for implementing this model T_c must be either provided or estimated somehow. To estimate the solar cell temperature, it is implemented the approach proposed by [61] which is based on the explicit Eq. (45):

$$T_c = T_a + POA \left[\exp(a_1 + a_2 V_w) + \frac{\Delta T_{ref}}{POA_{ref}} \right] \tag{45}$$

where V_w [m/s] is the free-stream wind speed measured at standard 10 m height; $\Delta T_{ref} = T_c - T_{back}$ is the temperature difference between the cell and the back surface of the module at STC (typically 2–3 °C according to [61]); $POA_{ref} = 1$ kW/m^2; and (a_1, a_2) are empirically determined coefficients which depend on the module construction, the mounting configuration, and the location and height where wind speed is measured. King et al. [61] provides a set of experimentally determined coefficients for flat-plate PV modules at different mounting configurations.

2.2.2.3. Walker model. Walker [55] proposed a model where the shunt resistance of the equivalent circuit is neglected based on the assumptions proposed by [83], thus the PV cell equivalent circuit for this model is as shown in Fig. 2(b), and its characteristic equation is (26). This simplification reduces the number of unknowns to four I_L, I_o, R_s and n. The author Walker [55] solved the problem by using an alternative analytical method based on the work of [67] which reduces the number of unknowns to just one, the series resistance (R_s). This approach is also implemented in [60,73,82]. The model considers the following effects:

a) Temperature dependence of the diode saturation current, I_o. Which is calculated using:

$$I_o = I_{o,ref} \left\{ \left(\frac{T_c}{T_{c,ref}} \right)^{\frac{3}{n}} \exp\left[\frac{E_g}{nk} \left(\frac{1}{T_{c,ref}} - \frac{1}{T_c} \right) \right] \right\} \tag{46}$$

The value of the saturation current at reference operating conditions ($I_{o,ref}$) is calculated assuming that at open-circuit condition $V = V_{oc,ref} \rightarrow I = 0 \rightarrow I_{L,ref} = I_{D,ref}$

$$0 = I_{L,ref} - I_{o,ref}\left[\exp\left(\frac{V + IR_s}{nkT_cN_s/q}\right) - 1\right] \quad \Rightarrow I_{L,ref} = I_{o,ref}\left[\exp\left(\frac{V + IR_s}{nkT_cN_s/q}\right) - 1\right] \tag{47}$$

At short-circuit condition $V = 0 \rightarrow I_{D,ref} = 0 \rightarrow I = I_{sc,ref}$

$$I = I_{sc,ref} = I_{L,ref} \tag{48}$$

Thus, from (46) and (48)

$$I_{o,ref} = \frac{I_{sc,ref}}{\left[\exp\left(\frac{V_{oc,ref}}{nkT_cN_s/q}\right) - 1\right]} \tag{49}$$

b) Temperature and radiation dependence of light current, I_L. Which is calculated using Eq. (33).
c) Internal losses due to current flow, represented through a series resistance, R_s.

The series resistance is known to have a very marked effect upon the slope of the I-V curve at $V = V_{oc}$. Hence if Eq. (26) is differentiated and evaluated at $V = V_{oc}$, the following expression in terms of R_s is found:

$$R_s = -\left[\left.\frac{dV}{dI}\right|_{V_{oc}} + \frac{1}{X_v}\right] \tag{50}$$

where,

$$X_v = I_{o,ref}\frac{q}{nkT_{c,ref}}\exp\left(\frac{V_{oc,ref}}{nkT_c/q}\right) \tag{51}$$

d) Leakage current losses to the ground are neglected, thus $R_{sh} = 0$.
e) One parallel diode with fixed ideality factor, n.

The model is now complete; all the constants present in Eqs. (46)–(51) can be obtained from the manufacturer's datasheet. It is worth mentioning that in order to compute R_s, the slope of the I-V curve at $[dV/dI]_{V_{oc}}$ is needed. Normally, this information is not included within the information provided in the datasheet, thus a graphic valuation must be carried out which is subjected to error [63]. This constitutes the main drawback of the Walker model [55]. Nevertheless, the practical simplicity of the model (no parameter extraction is needed) makes it useful when few information is available.

The net AC power delivered by the PV array, assuming it has a MPP tracker, is determined by Eq. (40), the inverter's efficiency is computed with the model presented in Section 2.3. The Walker model [55] also assumes that the cell temperature is known, thus in this work it is used Eq. (45) to estimate it from the ambient temperature.

2.3. Inverter models

Power conditioning equipment, such as inverters, constitute a key component in a PV system. They usually represent a small fraction in the total cost, but they influence to a great extent the performance of the system. Further, its reliability is critical for stand-alone applications. Frequently in modeling PV systems, the inverter efficiency is represented as a constant factor, which is the same of assuming the inverter's efficiency is linear over its operation range [61]. But in reality the inverter's efficiency, which indicates what fraction of the input power is transferred to the output, relies on the input voltage and on the load fraction at which the equipment is subjected [84]. Several approaches have been proposed to represent the electrical behavior of inverters, from simple efficiency approximations based on manufacturer datasheet information [56,84–87], empirically derived equations [88,89], to more complex analytical-based approaches to create an impedance model to simulate the frequency response of the inverter [90].

In the present study, it is implemented a model that is capable of representing the inverter's efficiency over the full range of operating conditions, simple to integrate in simulation tools and that produces results with good accuracy [84]. The model proposed by [91] and further improved by [87] fulfills these characteristics.

The efficiency of the inverter when referring to the input power (η_{inv}) of the device is given by:

$$\eta_{inv} = \frac{p - p_o - \kappa p^2}{p} \tag{52}$$

where p is the DC load fraction given by $p = P_{input}/P_{dc,rated}$; P_{input} is the DC input power; $P_{dc,rated}$ is the DC rated power; and

$$p_o = \frac{1}{99}\left(\frac{10}{\eta_{10}} - \frac{1}{\eta_{100}} - 9\right) \tag{53}$$

$$\kappa = \left(\frac{1}{\eta_{100}}\right) - p_o - 1 \tag{54}$$

Being η_{10} and η_{100} the inverter's efficiencies at 10% and 100% of the nominal power.

The parameters p_0 and κ are characteristic to each kind of inverter. The authors [87,92] define three type of inverters which represent the different possible "shapes" of the inverter's efficiency response. The type 1 inverter presents a lower efficiency for small load (< 30%), type 2 has the best efficiency whatever the percentage of load. Finally, the efficiency in type 3 decreases for high percentage of load in a more important way than for the two other types.

2.4. PV system losses

Performance losses one would expect in a real system and that are not explicitly modeled need to be specified as a percentage of the PV system power output [85]. These losses are normally represented by a derating factor which is a scaling factor that applies to the PV array power output to account for reduced output in real-world operating conditions compared to STC. They account for a series of non-temperature dependent losses such as [7,93]:

- DC losses: module nameplate DC rating; DC wiring; diodes and connections; mismatch; MPP tracker efficiency.
- AC losses: AC wiring; transformer.
- Other losses: soiling; shading; inverter; degradation; system availability; sun tracking and initial light-induced degradation (ILID).

The derating factors are normally derived from field measurements or estimations; they represent a negative impact on the PV system energy yield. Mondol et al. [94] presented a study where various roof mounted installations around the world were compared in terms of performance. The authors observed the difficulty in comparing different systems due to its variable characteristics, such as different design and orientation, climatic conditions, type of PV array and operating characteristic.

In Table 3 it is shown the range and typical values for the different derating factors aforementioned as reported by the cited references. The overall derating factor, f_{pv}, for a system is computed by multiplying the reduction due to each loss. The last column of Table 3 shows the values of the derating factors adopted in the present work to perform the simulations. The inverter's efficiency is not included in the system's derating factor, but rather considered as a separate input parameter.

Table 3
Derating factors for PV system modeling, range of variation and typical values reported in the literature.

		Reference						
		[103]		[85,109]		[7]		
	Derating factor	Range	Typical	Range	Typical	Range	Typical	Adopted
DC	Nameplate rating	0.85–1.05	1.00	0.80–1.05	0.95	–	0.95	0.95[d]
	DC wiring	0.97–0.99	0.98	0.97–0.99	0.98	–	–	0.98
	Diodes and connections	0.99–0.997	0.995	0.99–0.997	0.995	–	–	0.995
	Mismatch	0.97–0.985	0.98	0.97–0.985	0.98	–	0.98	0.98
	MPP tracker efficiency	–	–	–	–	0.98–1.00	0.99	0.99
AC	AC wiring	0.98–0.993	0.99	0.98–0.993	0.99	–	–	0.99
	Transformer	0.96 – 0.98	0.97	0.88–0.96[a]	0.92	–	0.98	1.00
Others	Soiling	0.75–0.98	0.95	0.30–0.995	0.95	–	–	0.98
	Shading	0.00–1.00	1.00	0.00–0.97	1.00	–	–	1.00
	Degradation (per year)	0.99–0.98	–	0.70–1.00	1.00	0.995–0.99	0.99	0.985
	System availability	0.00–0.995	0.98	0.00–0.995	0.98	–	–	1.00
	Sun tracking	0.98–1.00	1.00	0.98–1.00	1.00	–	–	1.00
	ILID	0.90–0.99	0.98[b]	–	0.985[c]	–	–	0.98
	Inverter	0.93–0.96	0.96	–	–			0.95[e]
	Overall f_{pv} at STC	0.62–0.92	0.80	–	0.77			0.842 0.80 (inverter)

[a] They combined the inverter and transformer efficiency into one DC–AC conversion factor.
[b] In concordance with [93].
[c] In concordance with [110].
[d] The nameplate rating derating factor does not apply for the equivalent-circuit-based models.
[e] Informed by manufacturer in the equipment datasheet as Euro-eta efficiency.

3. PV system in operation

The PV performance models were implemented and the result compared with a real 2.2 kWp PV system in operation, located in the Campus of the Otto-von-Güericke University (OvGU) in the city of Magdeburg, Germany. This system was installed in the year 2000 and it works to date injecting energy directly into the electrical system of the University.

3.1. PV array and Inverter

The PV array is mounted at the rooftop of the OvGU University building whose geographical location is 52°7′35″ North, 11°38′8″ East, GTM+1 and 72 m.a.s.l. The arrange is fixed mounted at 45° with respect to the horizontal, with an orientation of 12° respect to the true south. There are no obstacles nearby that can cast shadows on the panels. A 2 kVA rated inverter equipped with MPP tracker is used to condition the array's DC power output to AC form. The characteristics of the system's components are summarized in Table 4.

3.2. Measured data

A data acquisition system automatically performs hourly measurements of the following variables of interest: global horizontal irradiance (GHI), global irradiance on the plane of the array (POA), ambient temperature, module temperature, PV array DC power output and inverter's AC power output.

In order to get a full year of continuous hourly measurements for comparing the PV performance models, a 10-year time series collected by the data acquisition system was analyzed and verified for the existence of anomalies. The selected annual series corresponds to the year 2010, since it shows better consistency in the measurements over time.

In the case of irradiance data collected in a time steps of one hour, instrumental errors may be significant near sunrise and sunset hours, thus a quality control test to exclude spurious data needs to be conducted [95]. According to the methodology proposed by [96], all data that do not comply the following conditions should be filtered out:

$$\begin{cases} 0 \le DHI \le 1.1 \times GHI \\ 0 \le GHI \le 1.2 \times E_a \\ 0 \le DHI \le 0.8 \times E_a \\ 0 \le DNI \le E_a \end{cases} \quad (55)$$

After applying the conditions of Eq. (55), a total of 8761 hourly

Table 4
Characteristics of the PV module, PV array and inverter.

PV module		**PV array**	
Manufacturer/ model	Solarex MSX 110	Rated power	2200 Wp
Cell technology	poli-Si	Number of sub-arrays	1
Rated power	110 Wp	Number of modules in each sub-array	20
Configuration	12 V	Total number of modules	20
Number of cells in series	72	Total array area	20.5 m^2
Area	1.02292 m^2	Array open-circuit voltage	434 V
Current at MPP, I_{mp}	6.3 A	Array short-circuit current	6.9 A
Voltage at MPP, U_{mp}	17.5 V	Array voltage at MPP	336 V
Short-circuit current, I_{sc}	6.9 A	Array current at MPP	6.3 A
Open circuit voltage, U_{oc}	21.7 V	**Inverter**	
Temperature at NOCT	45 ± 2 °C	Manufacturer/ Model	SMA Sunny Boy 2000
Temperature coefficient of I_{sc}	4×10^{-4} 1/K	Max. DC power	2100 W
Temperature coefficient of U_{oc}	-3.4×10^{-3} 1/K	Max. AC power	2000 W
Temperature coefficient of P_{mp}	-1.943×10^{-4} 1/K	Max. AC apparent power	2000 VA
Efficiency at STC	10.75%	Efficiency	95%

measurements of the variables of interest were available to be used in the present work.

4. Results

In the present section, the accuracy of the predicted values calculated with the models presented in the previous sections with respect to the data measured at the PV system in operation is assessed. In order to disaggregate the errors of the PV performance model, the different submodels that comprise it are assessed separately. First, the accuracy of the POA irradiance models presented in Section 2.1 and then the accuracy of the PV performance model as a whole is studied. All the PV performance models were implemented in Matlab® computing language.

The adequacy of the models to predict the measured values was assessed with a series of statistical methods widely cited in the specialized literature [13,14,21,96–101]:

Mean bias error (MBE): provides information on the long-term performance of a model. A negative MBE value gives the average amount of underestimation in the calculated value, while a positive MBE means that the model tends to overestimate. One drawback of MBE is that overestimation of an individual observation may cancel underestimation in a separate observation [17,98]. The values of MBE and its relative form (rMBE) are obtained with the next equations:

$$MBE = \frac{\sum_{i=1}^{N}(y_i - x_i)}{N} \quad , \quad rMBE = \frac{\sum_{i=1}^{N}(y_i - x_i)}{N \cdot \bar{x}} \tag{56}$$

where y_i is the predicted (calculated) value, x_i is the observed measures, N the number of observations and where $\bar{x}$ is the measured mean value.

Root mean square error (RMSE): gives information on the short-term performance of the correlations by allowing a term-by-term comparison of the actual deviation between the predicted and measured values. The smaller the value is, the better the model's performance is, the equation of RMSE and its relative form (rRMSE) follows [46,98]:

$$RMSE = \sqrt{\frac{\sum_{i=1}^{N}(y_i - x_i)^2}{N}} \quad , \quad rRMSE = \sqrt{\frac{\sum_{i=1}^{N}(y_i - x_i)^2}{N}} / \bar{x} \tag{57}$$

R-squared (R^2): represents the proportion of variability in a data set that is accounted for by a model. Ideally, the value of R^2 calculated with Eq. (58) should be 1.

$$R^2 = 1 - \frac{\sum_{i=1}^{N}(y_i - x_i)^2}{\sum_{i=1}^{N}(x_i - \bar{x})^2} \tag{58}$$

4.1. Comparison between measured and estimated POA irradiance

The accuracy of the estimation of the amount of irradiance incident in the plane of the solar collector is of great importance since it may generate an uncertainty of up to 2% in the estimation of the PV system energy production [102].

The combination of the four decomposition models with the four transposition models presented in Sections 2.1.1 and 2.1.2 gives a total of 16 POA irradiance models. These 16 models were implemented and their estimations compared with the measured values.

The values of the statistical error indices are presented in Table 5. In terms of MBE, the models error ranges from −3.299 W/m^2 (−2.649% rMBE) for the OH-LJ model to 4.997 W/m^2 (4.013% rMBE) for the DIRINT-Pe model. While in terms of RMSE, the error ranges from 26.97 W/m^2 (21.66% rRMSE) for the OH-LJ to 19.21 W/m^2 (15.43% rRMSE) for the DIRINT-HDKR model. All of the models explain more than 98% of the variability with respect to the experimental values; the R^2 varies from to 0.9856 for the OH-LJ model to 0.9927 for the DIRINT-HDKR model.

Table 5
Statistical analysis of the POA irradiance models (decomposition model + transposition model) presented in Section 2.1. Values in bold signify the four best performing models in terms of lowest rMBE and rRMSE.

POA model	MBE (W/m^2)	rMBE (%)	RMSE (W/m^2)	rRMSE (%)	R^2	Order
OH+LJ	−3.299	−2.649	26.971	21.659	0.986	15
OH+Ko	−0.239	−0.192	26.451	21.241	0.986	10
OH+HDKR	2.377	1.909	22.326	17.929	0.990	8
OH+Pe	4.761	3.824	25.336	20.346	0.987	14
Er+LJ	−2.918	−2.343	25.588	20.548	0.987	12
Er+Ko	0.064	0.052	25.205	20.241	0.987	9
Er+HDKR	2.408	1.934	22.210	17.836	0.990	7
Er+Pe	4.548	3.653	25.360	20.365	0.987	13
DISC+LJ	**−1.176**	**−0.945**	**20.103**	**16.144**	**0.985**	**1**
DISC+Ko	**1.729**	**1.389**	**20.005**	**16.065**	**0.992**	**2**
DISC +HDKR	3.932	3.158	20.124	16.160	0.992	5
DISC+Pe	6.255	5.023	24.510	19.683	0.988	16
DIRINT+LJ	−2.392	−1.921	21.704	17.429	0.991	6
DIRINT +Ko	**0.606**	**0.487**	**21.269**	**17.080**	**0.991**	**3**
DIRINT +HDKR	**2.751**	**2.209**	**19.210**	**15.427**	**0.993**	**4**
DIRINT+Pe	4.997	4.013	23.252	18.673	0.989	11

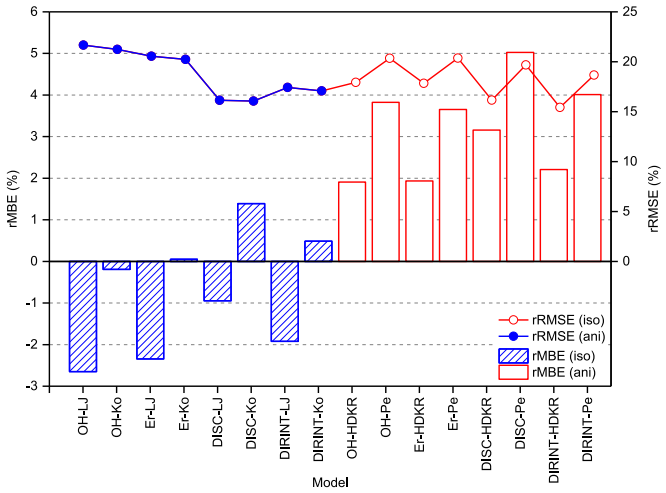

Fig. 3. Graphical comparison of the statistical errors for the POA irradiance models, grouped by isotropic sky (iso) and anisotropic sky (ani).

Fig. 3 presents a graphical representation of the rMBE and rRMSE of the combined irradiance models. Considering the rRMSE, the two isotropic transposition models (LJ and Ko) perform similarly, when combined either with the piecewise empirical decomposition models (OH and Er) or the quasi-physical decomposition models (DISC and DIRINT). On the other hand, the two anisotropic transposition models (HDKR and Pe) perform differently; the HDKR model shows lower values of rRMSE with respect to the Pe model when combined with any of the decomposition models.

Overall, the combined models that include an anisotropic sky transposition model tend to overestimate the POA irradiance (rMBE > 0). On the other hand, the combined models that include an isotropic model tend to underestimate the incident irradiance (rMBE < 0), with the exception of the Koronakis [23] model when combined with the Erbs et al. [18] (Er-Ko), the Maxwell [19] (DISC-Ko) and Ineichen et al. [20] (DIRINT-Ko) models. The fact that the isotropic transposition models underestimate the POA irradiance is related to the assumptions made in the models formulation. The isotropic models neglected the circumsolar diffuse and the horizon diffuse radiation fluxes, thus resulting in a lower amount of solar irradiance incident onto the plane

Table 6
Performance of the POA irradiance models according to the literature.

Reference	Site	Slope	Decomposition model	Transposition model	rMBE (%)	rRMSE (%)	Measured	Albedo
[111]	Castile and Leon region, Spain	42	–	LJ	−3.09	11.97	DNI, GHI	0.2
[112]	Geneva	30	–	LJ	−3.09	11.97	DNI, GHI	0.2
[100]	Ajaccio, Greece (LJ)	45	–	LJ	−8.9	12.77	DNI, GHI	0.2
[31]	Albany, NY, Trinity TX, USA	All	–	LJ	6.38	12.98	DNI, GHI	0.2
[35]	Finland	60	–	LJ	−8.7	16.80	DNI, GHI	0.2
[100]	Ajaccio, Greece (Ko)	45	–	Ko	−7.04	11.54	DNI, GHI	0.2
[100]	Ajaccio, Greece (Ko)	60	–	Ko	−3.63	11.37	DNI, GHI	0.2
[99]	Golden, Colorado, USA	40	Er	LJ	−5.2	12.50	GHI	0.2
[99]	Golden, Colorado, USA	40	Er	LJ	−4.8	11.90	GHI	Measured
[113]	Padova, Italy	20/ 30	Er	LJ	−2.38	8.52	GHI	0.2
[99]	Golden, Colorado, USA	40	DISC	LJ	−3.7	10.2	GHI	Measured
[31]	Albany, NY, Trinity TX, USA	All	–	HDKR	−0.12	8.16	DNI, GHI	0.2
[35]	Finland	30	–	HDKR	−4.3	9.20	DNI, GHI	0.2
[35]	Finland	60	–	HDKR	−3.3	11	DNI, GHI	0.2
[46]	Brussels, Belgium	50.79	–	HDKR	8.22	13.89	DNI, GHI	Measured
[100]	Ajaccio, Greece	45	–	HDKR	−10.901	19.25	DNI, GHI	0.2
[100]	Ajaccio, Greece	60	–	HDKR	−7.822	23.29	DNI, GHI	0.2
[99]	Golden, Colorado, USA	40	Er	HDKR	−1.9	8.30	GHI	0.2
[99]	Golden, Colorado, USA	40	Er	HDKR	−1.6	8.70	GHI	Measured
[113]	Padova, Italy	20/30	Er	HDKR	0.42	6.44	GHI	0.2
[99]	Golden, Colorado, USA	40	DISC	HDKR	−1.0	8.20	GHI	Measured
[100]	Ajaccio, Greece	45	–	Pe	−1.42	6.05	DNI, GHI	0.2
[114]	France, Carpentras	45	–	Pe	−1.03	3.60	DNI, GHI	0.2
[100]	Ajaccio, Greece	60	–	Pe	2.68	7.59	DNI, GHI	0.2
[35]	Finland	60	–	Pe	−2.5	9.30	DNI, GHI	0.2
[99]	Golden, Colorado, USA	40	Er	Pe	−1.6	10.40	GHI	0.2
[99]	Golden, Colorado, USA	40	Er	Pe	−1.2	10.10	GHI	Measured
[113]	Padova, Italy	20/30	Er	Pe	2.08	6.86	GHI	0.2
[99]	Golden, Colorado, USA	40	DISC	Pe	−0.5	9.80	GHI	Measured
[13]	Central, CO	40	DIRINT	Pe	0.4	8.00	GHI	0.2
[13]	Central, NM	35	DIRINT	Pe	0.5	5.00	GHI	0.2
This work	Magdeburg, Germany	45	DISC	LJ	−0.945	16.14	GHI	0.2
This work	Magdeburg, Germany	45	DISC	Ko	1.389	16.06	GHI	0.2
This work	Magdeburg, Germany	45	DIRINT	Ko	0.487	17.08	GHI	0.2
This work	Magdeburg, Germany	45	DIRINT	HDKR	2.209	15.42	GHI	0.2

of the array.

A literature review was performed, and the values of POA irradiance models error reported by other authors are shown in Table 6. According to Table 6, the rRMSE for the POA irradiance models vary from 5% for a combined DIRINT-Pe model [13] to 23.29% for a model that computes the POA irradiance from the HDKR transposition model and measured DHI and DNI [100]. The last four lines of Table 6 present the combined models that performed better in the present study: DISC-LJ, DISC-Ko, DIRINT-Ko and DIRINT-HDKR. The rMBE and rRMSE of these models are in line with the values reported by other authors, thus, these four POA irradiance models are used in the PV performance models in the following sections.

Predicted values of POA irradiance (hourly values) for the four best models found in the present work are compared with measured values, the plots are shown in Fig. 4. The straight dashed lines corresponds to the predicted values being equal to the predicted ones, while the solid line is the best linear fit of the data.

4.2. Comparison between measured and estimated PV system power output

Once the incident irradiance in the plane of the array is known, the next step consists in estimating the PV system power output, i.e. the AC power generated by the PV array under the specific operational conditions. This is done by combining the POA irradiance submodel, the PV module submodel, the inverter submodel and the non-temperature dependent losses into one PV system performance model.

A total of 20 PV performance models are studied which derive from the combination of the four best POA irradiance models obtained in Section 4.1 and the five PV module models presented in Section 2.2. The values predicted by the PV performance models are compared with values measured from the real 2.2 kWp PV system.

To be consistent with the losses, the same derating factor for all the PV performance models is assumed. It is worth mentioning that for the equivalent-circuit-based module models (De Soto et al., Villalva et al. and Walker), it is not applicable the “name plate rating” derating factor (see Section 2.4), because the real rated power of the module is estimated when extracting the parameters of the characteristic equation instead of using the rated power provided by the manufacturer in the datasheet. Considering the above mentioned and using the derating factors listed in Table 3, the overall derating factor resulted in $f_{pv} = 0.842$ for the power module models and $f_{pv} = 0.886$ for equivalent-circuit-models based module models.

The results of the statistical analysis are summarized in Table 7 for the 20 PV performance models implemented. Overall, the MBE varies from −23.985 W (−10.854% rMBE) for the Villalva+DISC+LJ model to 14.178 W (6.416% rMBE) for the HOMER+DIRINT+Ko model. In terms of RMSE the error ranges from 33.364 W (15.099% rRMSE) for the DeSoto+DIRINT+Ko model to 54.932 W (24.859% rRMSE) for the Villalva+DISC+LJ.

It is observed in Table 7 that the PV performance models that incorporate a power module model (Diaf et al. and HOMER) tend to overestimate the PV system power output, given the positive value of rMBE. On the other hand, all the PV performance model that incorporate an equivalent-circuit-based module model (De Soto et al., Villalva et al. and Walker) tend to overestimate the power output, resulting in negative values of rMBE. The average rMBE of all the power models and the equivalent-circuit-based models resulted similar, although different in sign, 5.14% for the former ones (overestimation) and −4.91% (underestimation) for the later ones. In terms of average rRMSE, the power models performed slightly better (17.09% average rRMSE) than the equivalent-circuit-based models (20.32%

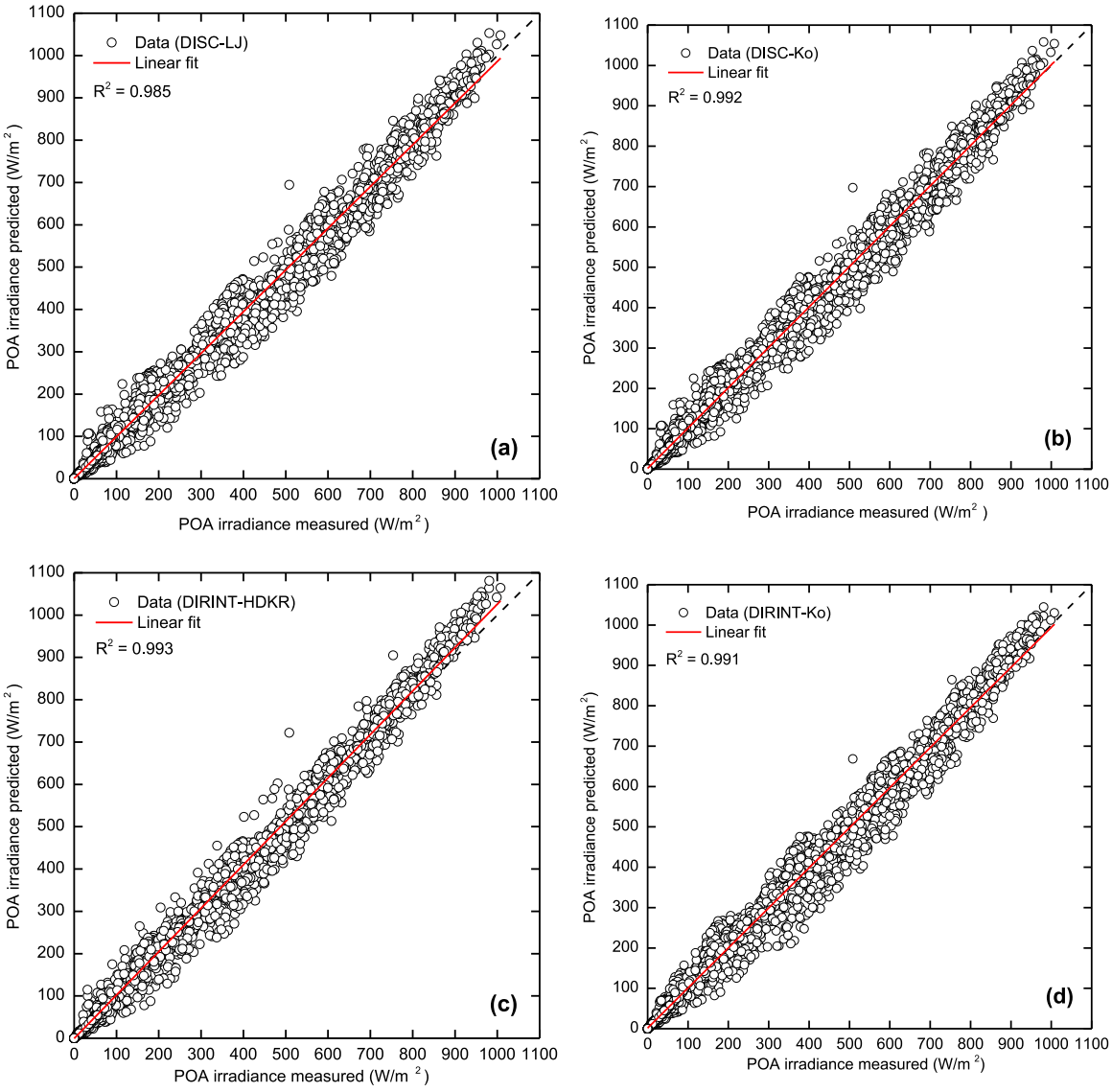

Fig. 4. Predicted and measured POA irradiance of the four best decomposition-transposition combined models: (a) DISC-LJ, (b) DISC-Ko, (c) DIRINT-HDKR and (d) DIRINT-Ko.

average rRMSE). Among all the models implemented the one that performed better in terms of lowest rMBE and rRMSE, is the DeSoto +DIRINT+Ko model, while the worst performing model is the Villalva +DISC+LJ model.

In order to compare the results obtained here with other values reported, a literature review on related works was performed. It is worth mentioning that few works can be found that assess the long term performance of PV performance models by comparing the estimated values with experimental or field measurements. Further, these works report the model error using different metrics, thus making difficult the use of the results for comparison purpose. Most of the reported values are expressed in terms of bias error or total difference between estimated and measured values, which gives little information about the accuracy of the PV system performance model. Table 8 summarizes the results of the literature review on works that assess the performance of PV system models using experimental data. Most of the works employ commercial simulation software to perform the analysis, among them: SAM, PVSyst, PVSol, PVWatts, HOMER, RETScreen, PVDesign-Pro and TRNSYS [11]. All of them report the model error in terms of rMBE and only one author provides the rRMSE of the estimated values [10]. The bulk of the PV performance models combine an anisotropic sky transposition model, HDKR or Perez et al. (Pe), with an equivalent-circuit-based PV module model, CEC 5-parameter [61] or Sandia [61].

The rMBE reported by authors shown in Table 8 vary from −15.2–23.8%, while the rRMSE reported by [10] ranges from 6.5–9.7%. It is worth mentioning that most of the models use irradiance data of two components GHI and DHI or GHI and DNI, thus the error of the simulation is reduced because there is no need of decomposition model. The values of rMBE obtained in the present work (Table 7) are in line with the values reported in the literature (Table 8). The values of rRMSE found here exceeds the values reported by the only reference that provided this error [10].

4.2.1. Analysis of best PV performance models

The bold values in Table 7 correspond to the PV system models that performed better for each combination of PV module model and the best four POA irradiance models, these are: (1) Diaf+DISC+LJ; (2) HOMER+DISC+LJ; (3) DeSoto+DIRINT+Ko; (4) Villalva+DIRINT +Ko and (5) Walker+DIRINT+Ko. These five models are studied in more detail following.

A series of performance indices are computed; these indices are related to the annual DC and AC energy yield of the PV system, the PV array efficiency, the inverter's efficiency, the temperature of the solar cell and the Performance Ratio (PR), which is an energy quality factor used to compare PV power plants [103]. A statistical analysis is also

Table 7
Statistical analysis on the PV performance models implemented, combination of PV module model+decomposition model+transposition model.

	MBE (W)	rMBE (%)	RMSE (W)	rRMSE (%)	Order
Power models					
Diaf+DIRINT+Ko	12.322	5.577	35.076	15.874	8
Diaf+DIRINT+Re	10.110	4.575	39.546	17.896	10
Diaf+DISC+LJ	**7.866**	**3.560**	**37.919**	**17.160**	**5**
Diaf+DISC+Ko	11.570	5.236	39.644	17.941	12
HOMER+DIRINT +Ko	14.178	6.416	35.281	15.967	9
HOMER+DIRINT +Re	11.871	5.372	38.721	17.523	11
HOMER+DISC +LJ	**9.597**	**4.343**	**36.806**	**16.657**	**7**
HOMER+DISC +Ko	13.357	6.045	39.040	17.668	13
Average	11.359	5.14%	37.754	17.09%	
Equivalente-circuit-based models					
DeSoto +DIRINT+Ko	**−0.445**	**−0.201**	**33.364**	**15.099**	**1**
DeSoto+DIRINT +Re	−2.530	−1.145	40.654	18.398	3
DeSoto+DISC+LJ	−4.678	−2.117	40.646	18.394	4
DeSoto+DISC+Ko	−1.116	−0.505	39.670	17.953	2
Villalva +DIRINT+Ko	**−19.748**	**−8.937**	**45.176**	**20.444**	**17**
Villalva+DIRINT +Re	−22.017	−9.964	53.214	24.082	19
Villalva+DISC+LJ	−23.984	−10.854	54.932	24.859	20
Villalva+DISC+Ko	−20.611	−9.328	51.043	23.100	18
Walker +DIRINT+Ko	**−7.074**	**−3.202**	**39.229**	**17.753**	**6**
Walker+DIRINT +Re	−9.105	−4.120	47.194	21.358	15
Walker+DISC+LJ	−11.179	−5.059	47.884	21.670	16
Walker+DISC+Ko	−7.734	−3.500	45.761	20.709	14
Average	−10.852	−4.91%	44.897	20.32%	

performed over the results of the simulations and the MBE, RMSE and R^2 of the performance indices aforementioned is calculated. The results are summarized in Table 9.

The first performance index is the PV DC annual yield that indicates the PV system power generation for the period of simulation (one year in this case), measured before the inverter. The DC annual yield values estimated by the models in Table 9 comprise the uncertainty of the POA irradiance model, the module model and the DC losses. With exception of the Villalva+DIRINT+Ko and the Walker+DIRINT+Ko, all the models tend to overestimate the DC power output, resulting in a positive MBE. The DeSoto+DIRINT+Ko model presents the best accuracy in terms of rMBE (0.704%) and rRMSE (13.645%). In consequence, the PV array efficiency estimated by this model result closer to the efficiency of the real system. The Villalva+DIRINT+Ko model is the worst performing model in terms of DC power output, with a rMBE of −8.148% and rRMSE of 18.649%.

The next index shown in Table 9 is the PV AC annual yield, which accounts for the power generation for the period of simulation after the inverter. The PV system models that incorporate an equivalent-circuit-based module model tend to sub estimate the annual AC energy production, while the power models overestimate the AC annual yield. The rMBE ranges from −8.937 to 4.343% and the rRMSE from 15.099% to 20.444%.

The PV system models that incorporate the power module models proposed by HOMER and Diaf et al. performed comparably well with respect to the equivalent-circuit-based module models, considering the simplified approach they propose. Further, these models performed better than the Villalva et al. and Walker equivalent-circuit-based-models in terms of rRMSE.

All and all, the best PV performance model is the one that combines the De Soto el al. [52] PV module model, the DIRINT [20] decomposition model, the Koronakis [23] isotropic sky irradiance model, and the Schmid and von Dincklage [91] inverter model. This PV performance model estimated the AC annual yield with the lowest rRMSE (15.099%) and negligible rMBE (−0.201%), meaning that the model tends to compensate the error along the year.

The Schmid and von Dincklage [91] type 3 inverter model predicts the measured data with good accuracy, the percentage error with respect to the measured inverter's efficiency ranges from −0.899% to −0.843%. This demonstrates that the inverter's efficiency curve can be well represented by a simple quadratic function, though smaller errors can be achieved by using a double quadratic function as reported by [84]. The single point approach to represent the efficiency of the inverter used in Diaf+DISC+LJ and HOMER+DISC+LJ models results in a greater percentage of error (3.115%) when considering the nominal efficiency reported by the manufacturer in the inverter's datasheet. In the single point approach, the error may be reduced if experimental data of the inverter's efficiency is available prior to the simulations.

All the models fail to accurately estimate the cell temperature. The rRMSE ranges from 18.550% up to 36.914%. The HOMER and Diaf et al. power models neglect the effect of wind speed in the estimation of the cell temperature, thus the error results higher. Previous works [81] have emphasized the importance of the correlations used to estimate the temperature of the solar cell, and how this depends on the module installation conditions and the geographic location system. This constitutes an important aspect were the PV module models need to be improved.

The performance ratio (PR) index includes all the uncertainties in the PV system modeling chain. In our case, it includes the POA irradiance model uncertainty, the PV module model uncertainty (which includes the cell temperature estimation) and the non-temperature related losses uncertainty. The Diaf+DISC+LJ and HOMER+DISC+LJ models tend to overestimate the PR with a difference of 3.560% and 4.343%, respectively; the Villalva+DIRINT+Ko and Walker+DIRINT +Ko models tend to underestimate the PR with a difference of −8.937% and −3.202%, respectively; the DeSoto+DIRINT+Ko model accurately estimates the PR with a difference of −0.201%.

It is worth mentioning that even DeSoto+DIRINT+Ko model presents the best accuracy, the computer time required for the simulation resulted much higher with respect to the other models, as observed in the last line of Table 9. Using a computer equipped with Windows 7 64 Bits, processor Intel Core i7 2,5 GHz and 8 GB of RAM, the DeSoto+DIRINT+Ko model took 71.774 s, while fastest algorithm, the HOMER+DISC+LJ models, took 0.032 s. The DeSoto+DIRINT+Ko model is time consuming due to the De Soto et al. module model recalculates the parameters of the solar cell equivalent circuit for every new operating condition, i.e. for every time step, which in our case was 8760 h. If the model needs to be used to iteratively simulate a PV system, such is the case of an optimization algorithm, the computational cost may constitute a decisive factor for choosing the most appropriate model to be implemented.

A general approach to validate a PV system simulation model is to generate a scatter plot of predicted power vs. measured power for each time interval (one hour in the present study) [104]. The scatter plots for the five PV system performance models presented in Table 9 are shown in Figa. 5(a)–9(a). The blue dashed line has a slope of 1 and represents exact equality between measured and modeled values. Points that fall above the line indicate that the model is overestimating power from the array and points below the line indicate that the model is underestimating power. The red solid line represents the linear fit of the points, showing the trend of the model with respect to the measured values. In all the models, the dispersion of points is higher for lower levels of PV power output (< 500 W); this indicates that the models fail do accurately represent the PV system behavior during

Table 8
Literature review on the PV performance models estimated error.

Ref.	PV system	Decomposition model	Transposition model	PV Module model	rMBE (%)	rRMSE (%)	Irradiance data
[115]	205 kW rooftop, Washington, USA	–	HDKR	Sandia[61]	2.41	–	GHI, DNI
		–	HDKR	Sandia[61]	−0.11	–	GHI, DHI
		–	Pe	Sandia[61]	2.41	–	GHI, DNI
		–	Pe	Sandia[61]	−0.22	–	GHI, DHI
		–	Pe	CEC 5-parameter[61]	−0.67	–	GHI, DNI
		–	Pe	CEC 5-parameter[61]	−3.06	–	GHI, DHI
[8]	Six systems 5–7 kW, Alice Spring, Australia	Er	HDKR	HOMER power model	−1.44	–	GHI
		Er	HDKR	PVsyst one diode equivalent-circuit model	−4.33	–	GHI
		Er	LJ	RETScreen power model, based on[51]	−2.31	–	GHI
[7]	78.4 kW rooftop Escondido, USA	Er	HDKR	PVsyst one diode equivalent-circuit model	−2.6	–	GHI
		–	Pe	CEC 5-parameter[61]	3.3	–	GHI, DHI
		–	Pe	PVWatts power model[61]	−2.5	–	GHI, DHI
		Reindl et al.[27]	HDKR	PVSol one diode equivalent-circuit model[61]	−6.8	–	GHI, DHI
		–	Pe	Sandia[61] implemented in PVDesign-Pro	−3.7	–	GHI, DHI
	481.5 kW ground-mounted, Santee, USA	Er	HDKR	PVsyst one diode equivalent-circuit model	−8.2	–	GHI
		–	Pe	CEC 5-parameter[61]	−3.0	–	GHI, DHI
		–	Pe	PVWatts power model[61]	−8.5	–	GHI, DHI
		Reindl et al.[27]	HDKR	PVSol one diode equivalent-circuit model[61]	−10.6	–	GHI, DHI
		–	Pe	Sandia[61] implemented in PVDesign-Pro	−15.2	–	GHI, DHI
[10]	1.1 kW Albuquerque, USA	–	Pe	CEC 5-parameter[61]	9.1	9.4	GHI, DHI
		–	Pe	Sandia[61]	5.4	6.6	GHI, DHI
		–	Pe	PVWatts power model[61]	10.2	7.0	GHI, DHI
	2.3 kW Albuquerque, USA	–	Pe	CEC 5-parameter[61]	8.5	6.5	GHI, DHI
		–	Pe	Sandia[61]	3.6	8.0	GHI, DHI
		–	Pe	PVWatts power model[61]	9.6	9.7	GHI, DHI
[116]	13 kW Northren Ireland	Reindl et al.[27]	LJ	TRNSYS one diode equivalent-circuit model[117]	15.8	–	GHI
		Site specific correlation	LJ	TRNSYS one diode equivalent-circuit model[117]	5.9	–	GHI
		Reindl et al.[27]	Hay and Davies [34]	TRNSYS one diode equivalent-circuit model[117]	23.8	–	GHI
		Site specific correlation	Hay and Davies [34]	TRNSYS one diode equivalent-circuit model[117]	13.9	–	GHI
[107]	Nine commercial scale systems (< 1 MW), USA	–	Pe	CEC 5-parameter[61]	−5.0 to 4.1	–	DNI, DHI
		Er	Pe	PVsyst one diode equivalent-circuit model	−1.7 to 5.5	–	GHI
		Reindl et al.[27]	HDKR	PVSol one diode equivalent-circuit model [61]	−5.5 to 1.4	–	GHI
		–	Pe	PVWatts power model [61]	−16.2 to −8.9	–	DNI, DHI

periods of low irradiance levels. At higher levels of power production (> 750 W), the models tend to underestimate the power output, given that the linear fit line falls below the slope 1 line. This effect is less evident for the Diaf+DISC+LJ (Fig. 5(a)), HOMER+DISC+LJ (Fig. 6(a)), and DeSoto+DIRINT+Ko (Fig. 7(a)) models, while for the Villalva+DIRINT+Ko (Fig. 8(a)) and Walker+DIRINT+Ko (Fig. 9(a)) models the bias is market. The bias in the models may be reduced by adjusting the value of the derating factor that multiplies the power predicted by the model, this is discussed in the next section.

Other useful analysis to validate a PV performance model is to examine the distribution of model residuals, $e_i = y_i - x_i$, with the help of a histogram. Fig. 5(b) to Fig. 9(b) present the histogram of residuals for the five PV system performance model presented in Table 9. Ideally, the distribution of residual should present a normal distribution, as the best fitted normal probability function plotted in red in the figures. A slight skewness is common due to the high frequency of residual close to zero. This is an expected behavior because there are two moments of low irradiance during the day, and therefore the residuals have low absolute value.

4.3. Uncertainties in the PV performance models

An average percentage difference of the estimated results to the actual energy yield of around 5% is considered acceptable for feasibility studies [8]. But, as demonstrated by [105] the combined uncertainty of the annual yield of a PV system may rise up to 8.7% for individual years, and up to 7.9% for the average yield over the system's lifetime. The reference [6] reported that the use of the best available PV performance algorithms result in uncertainties in the order of ± 3.75% to ± 5%, not considering the uncertainties of the non-tempera-

Table 9
Statistical analysis of the five best PV performance models implemented in the present work.

		Measured	Power models		Equivalent-circuit-based models			
			Model 1	Model 2	Model 3	Model 4	Model 5	
			Diaf et al.	HOMER	De Soto et al.	Villalva et al.	Walker	PV module model
			DISC	DISC	DIRINT	DIRINT	DIRINT	Decomposition model
			LJ	LJ	Ko	Ko	Ko	Transposition model
DC mean output	W	239.845	243.053	244.878	241.5334	220.302	234.140	
DC annual yield	kWh	2072.503	2100.222	2115.963	2087.099	1903.632	2023.204	
MBE	W		3.208	5.030	1.689	−19.543	−5.705	
rMBE	%		1.337	2.097	0.704	−8.148	−2.379	
RMSE	W		41.833	39.768	32.726	44.729	38.350	
rRMSE	%		17.442	16.581	13.645	18.649	15.989	
Rsquared			0.991	0.992	0.995	0.990	0.993	
PV array efficiency	%	9.415	9.541	9.612	9.481	8.648	9.191	
Percentage error	%		1.337	2.097	0.704	−8.148	−2.379	
AC mean output	W	220.970	228.835	230.566	220.525	201.222	213.895	
AC annual yield	kWh	1905.553	1977.367	1992.320	1905.553	1738.756	1848.267	
MBE	W		7.866	9.597	−0.445	−19.748	−7.074	
rMBE	%		3.560	4.343	−0.201	−8.937	−3.202	
RMSE	W		37.919	36.806	33.364	45.176	39.229	
rRMSE	%		17.160	16.657	15.099	20.444	17.753	
Rsquared			0.992	0.993	0.995	0.998	0.995	
Inverter Efficiency	%	92.130	95.000	95.000	91.302	91.339	91.353	
Percentage error	%		3.115	3.115	−0.899	−0.859	−0.843	
Mean cell temperature	°C	11.683	14.898	14.427	13.046	14.037	14.037	
MBE	°C		3.214	2.743	1.362	2.354	2.354	
rMBE	%		27.512	23.480	11.659	20.148	20.148	
RMSE	°C		4.313	3.502	2.167	2.849	2.849	
rRMSE	%		36.914	29.975	18.550	24.386	24.386	
Rsquared			0.897	0.932	0.974	0.955	0.955	
PR = Yf/Yr		0.807	0.835	0.842	0.805	0.735	0.781	
Yf	h	867.908	898.803	905.600	866.161	790.344	840.122	
Yr	h	1076.017	1076.017	1076.017	1076.017	1076.017	1076.017	
Percentage error	%		3.560	4.343	−0.201	−8.937	−3.202	
Simulation time	s		0.040	0.032	74.774	21.592	32.241	

ture dependent losses present in the system.

However the error values differ depending on the reference consulted, they are useful for comparison with the values obtained in the present work. According to the results shown in Table 9, with exception of the Villalva+DIRINT+Ko model, all the models present a level of accuracy of ± 5% rMBE and less.

A series of errors in the modeling chain contribute to the deviation of the estimations from the measured values. The first source of error derives from the underlying mathematical algorithms used in the simulations. These include the error of the POA solar irradiance models, the error of the PV module models (which includes the estimation of the solar cell temperature), and error of the inverter models; all these were discussed in Sections 4.1 and 4.2.

Another important source of error, that influences critically the accuracy of the models, proceeds from the uncertainty in the estimation of the non-temperature dependent losses. These estimates can be handled with varying levels of complexity. In the present study, it is adopted the approach of using a single non-temperature global derating factor (f_{pv}) to encapsulate the many possible reduction factors (losses) exposed in Section 2.4. For the PV system studied in present

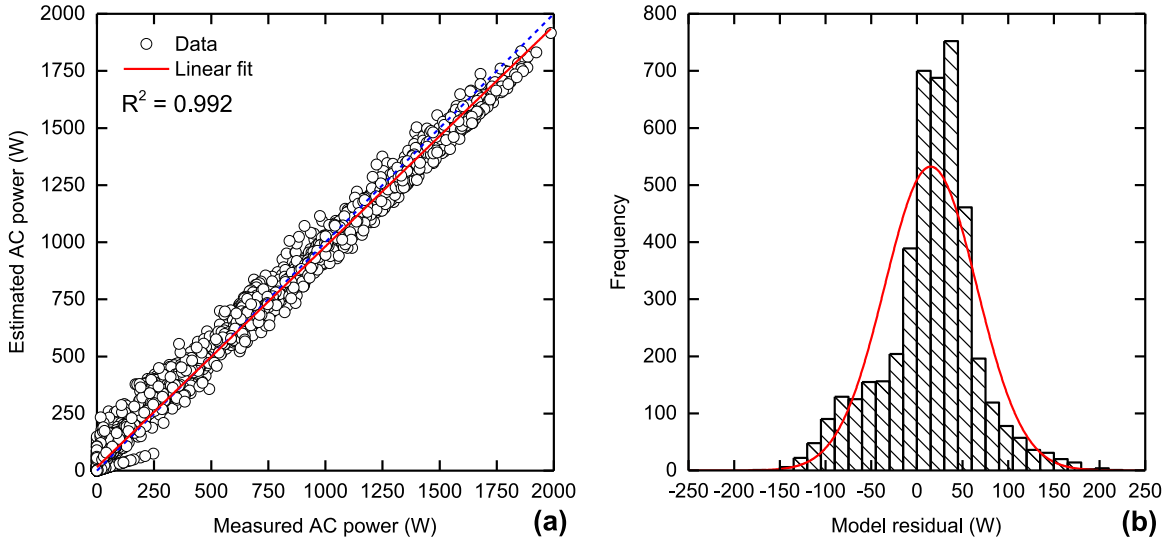

Fig. 5. Scatter plot of predicted vs. measured AC power output (a), and histogram of residuals (b) for the Diaf+DISC+LJ model.

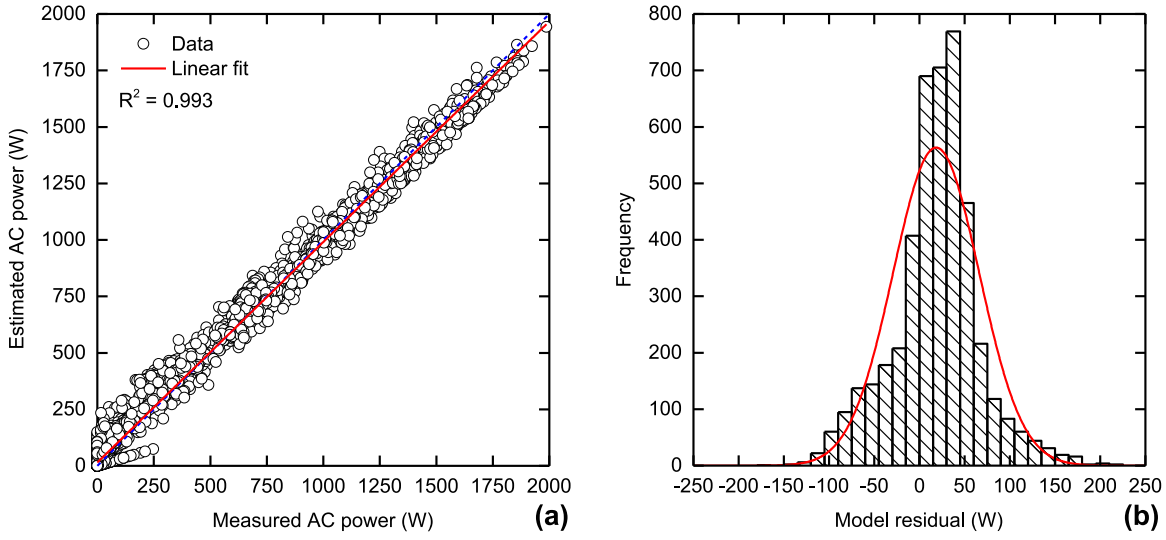

Fig. 6. Scatter plot of predicted vs. measured AC power output (a) and histogram of residuals (b) for the HOMER+DISC+LJ model.

work, the estimated value of global derating factor resulted in f_{pv} =0.842 for the power module models and f_{pv}=0.961 for the equivalent-circuit-based models, which is in the range recommended by [106]. Losses considered by this reduction factor are not easily measurable, not much information is available in the literature on this subject and there is a big spread within the values reported. Some authors have observed the difficulty in estimating a single value of derating factor to be used in any situation due to the great dependency on the PV system characteristics [94]. A good study on the influence of the uncertainties related to the variables involved in PV system modeling can be found in [105]. The authors comment that the uncertainty could be further reduced by moving to more accurate module rating and learning to better estimate losses due to dirt, soiling and snow. Another study published by [107] suggests that expert PV system modelers may have information and experience to make more accurate loss assumptions for a given system; however, the data to make these assumptions is lacking in the industry sector as a whole. In short, the estimates and assumptions will finally rely on the criterion of the PV modeler and are highly dependent on its experience.

In order to study the influence of the uncertainty of the derating factors on the predicted PV system power output, a probabilistic simulation was performed. This was implemented using the Latin Hypercube Sampling (LHS) [108] method to probabilistically generate samples of the individual derates and combine them into the global derating to be used in the PV system simulation. The uncertainty of the derating factors shown in Table 3 was extracted from the work of [105], which provides the next values: nameplate rating ±3%; dirt, soiling and snow ±5%; others (DC/AC wiring, diodes and connections, mismatch, MPPT efficiency, shading, degradation and ILID) ±5%. The results of the probabilistic simulation for the five PV performance systems are presented in Fig. 10 in the form of histograms. These graphs provide information about the degree of influence of the derating factors uncertainty over the rMBE of the PV system AC power production, the dashed line represents the rMBE obtained with the derating factors adopted in the present study.

It is observed that an incorrect choice of the derating factors may lead to significant errors in the estimated energy yield of the PV system, more than 30% of rMBE in some scenarios. The PV performance models that include the power module models, Fig. 10(a) and (b), show a tendency to overestimate the PV power output, while in the case of the equivalent-circuit-based module models, Fig. 10(c), (d) and (e) the tendency is to underestimate the power output, this effect is more pronounce if the wrong choice of derating factors is made. The PV expert who is assessing the performance of an existing system must possess the necessary information in order to properly assign the derating factors. Likewise, in case a new PV system is being projected,

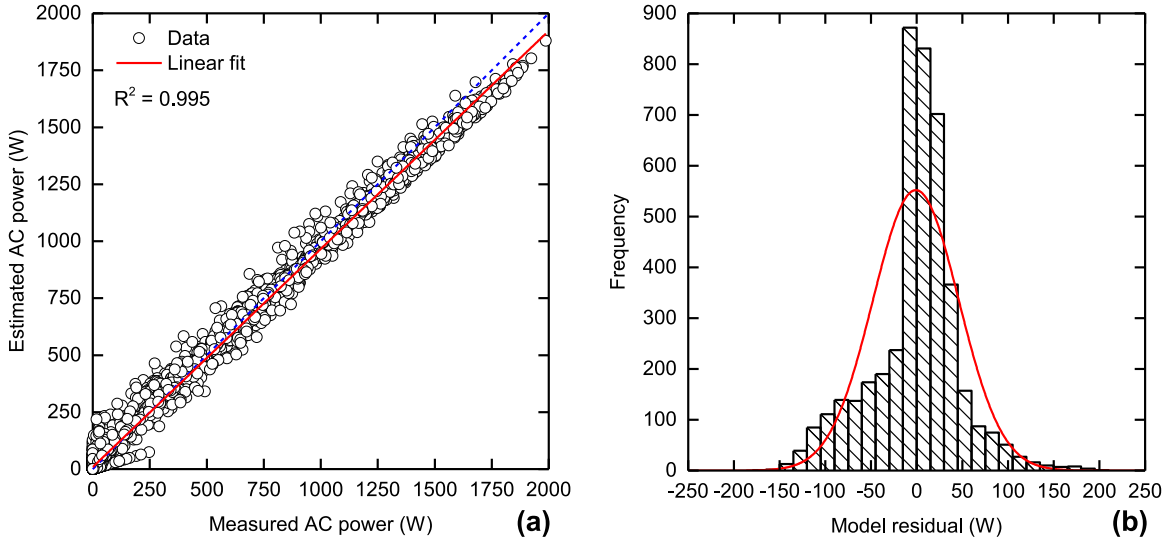

Fig. 7. Scatter plot of predicted vs. measured AC power output (a) and histogram of residuals (b) for the DeSoto+DIRINT+Ko model.

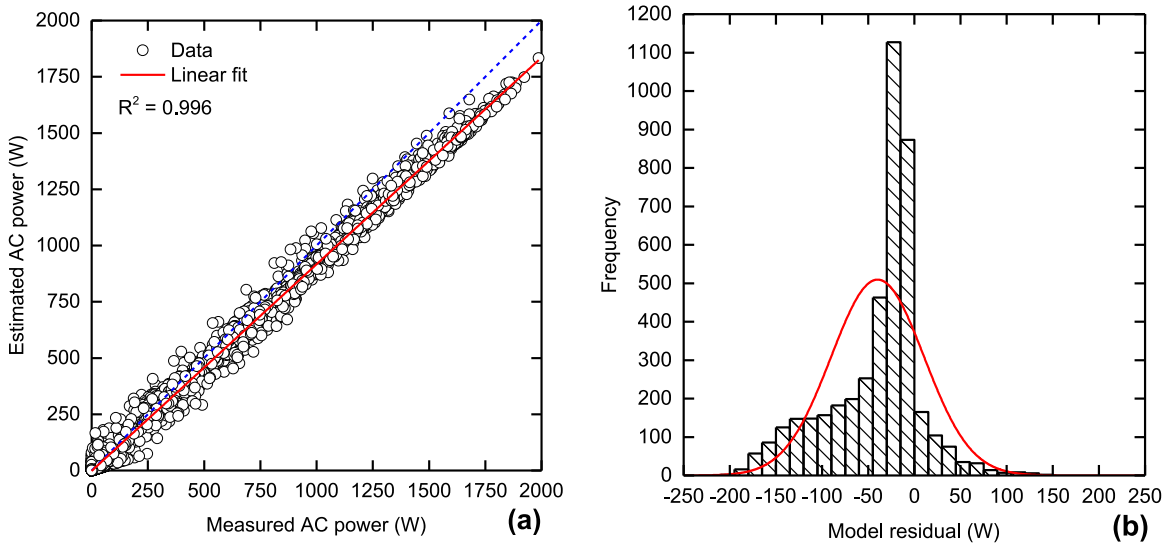

Fig. 8. Scatter plot of predicted vs. measured AC power output (a) and histogram of residuals (b) for the Villalva+DIRINT+Ko model.

the annual yield estimations would apply exclusively to the specified operating conditions at which the system was modeled and with the derates adopted.

5. Conclusion

The modeling process of a PV system involves two main stages, the estimation of the incident irradiance in the POA and the estimation of the PV module output power. For each of these steps, different models are available in the literature. The main objective of the present work is to assess the performance of different combinations of the most cited models aiming to find a PV performance model with good accuracy. To do so, 16 combinations of decomposition-transposition models were implemented in order to select the four best POA irradiance models. The POA combined models that performed better are: DISC-LJ, DISC-Ko, DIRINT-Ko and DIRINT-HDKR. They presented a rMBE between −0.945% and 2.209% and a rRMSE between 15.42% and 17.08%, which is in line with the values reported by other authors.

The four best POA irradiance models were then combined with five PV module models, two of the type power models, and three equivalent-circuit-based models, and two inverter models, a single point efficiency and a quadratic fitting function, resulting in 20 PV system performance models. Their performance was compared with monitored data derived from a real 2.2 kWp PV system in order to assess its accuracy.

It is observed that the PV performance models that incorporate a power module model (Diaf et al. and HOMER) tend to overestimate the PV system power output, with an average rMBE of 5.14%, while the PV performance models which incorporate an equivalent-circuit-based module model (De Soto et al., Villalva et al. and Walker) tend to underestimate the power output with an average rMBE of −4.91%. Overall, the PV performance model with the highest accuracy is the combination of the DIRIN [20] decomposition model, the Koronakis [23] transposition model, the De Soto el al. [52] PV module model and the Schmid and von Dincklage [91] inverter model. This PV performance model presents the lowest error with respect to the AC power output, with a rMBE of −0.201% and a rRMSE of 15.099%.

Several sources of error were identified in the PV performance models that result in a difference between the true values of the values predicted by the simulation. The first source of error to be considered is the one derived by the underlying mathematical algorithms used in the simulations. Another critical source of error derives from the uncertainty in the determination of the global derating factor, which is a power reduction factor that accounts for the non-temperature depen-

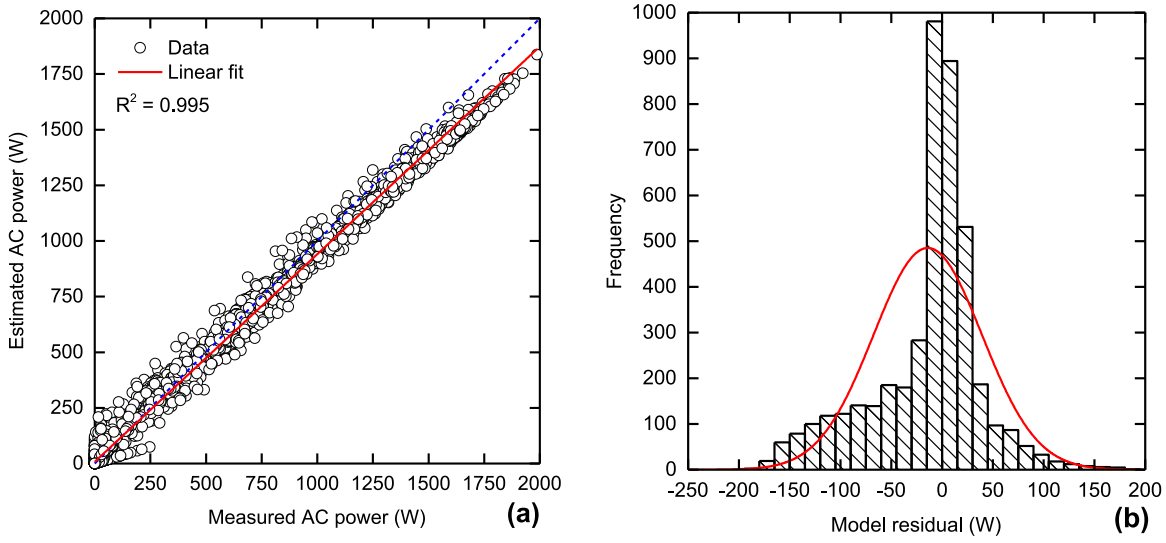

Fig. 9. Scatter plot of predicted vs. measured AC power output (a) and histogram of residuals (b) for the Walker+DIRINT+Ko model.

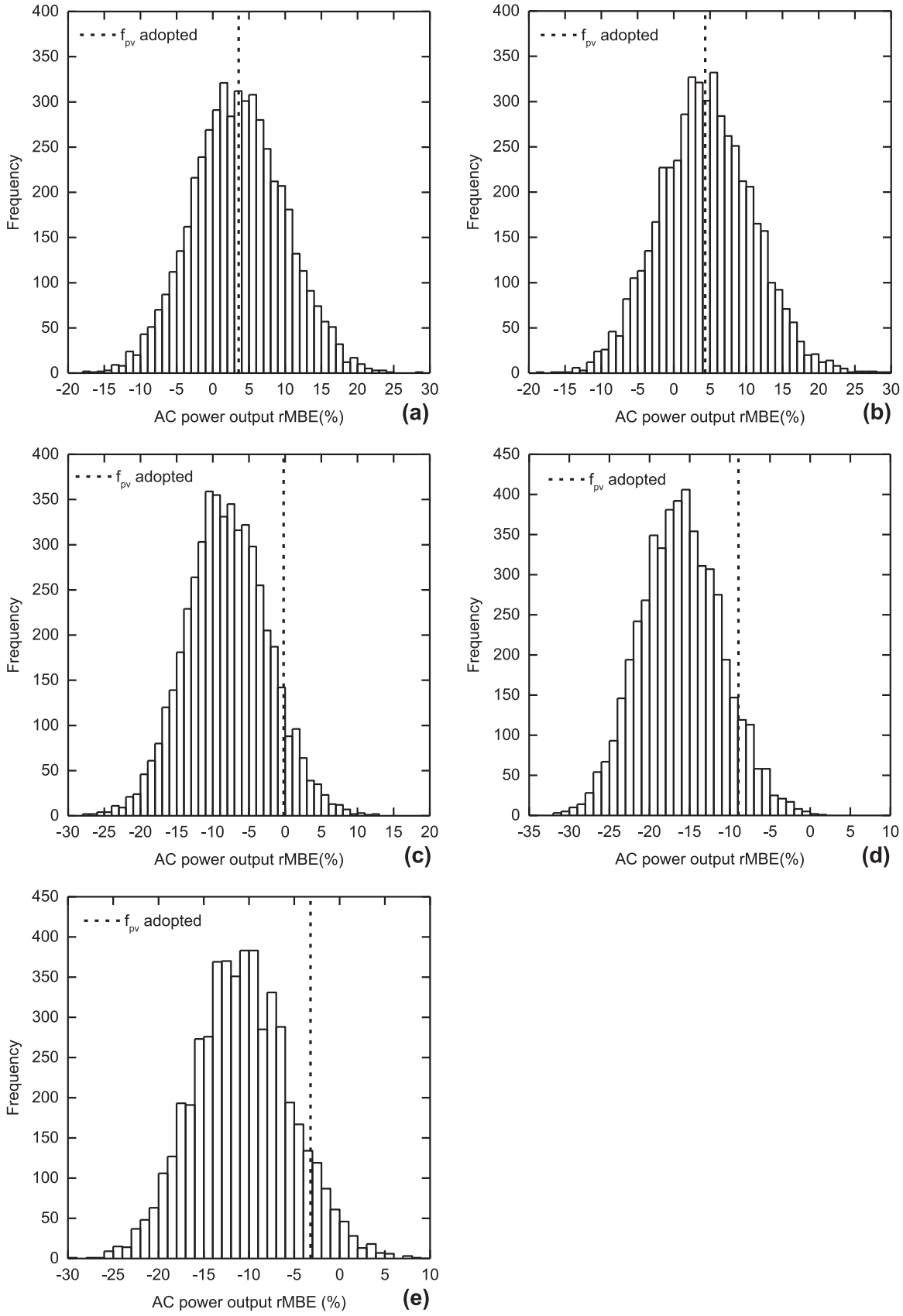

Fig. 10. Influence of the derating factor (f_{pv}) uncertainty over the AC power output rMBE: (a) Diaf-DISC-LJ, (b) HOMER-DISC-LJ, (c) DeSoto-DIRINT-Ko, (d) Villalva-DIRINT-Ko, (e) Walker-DIRINT-Ko.

dent losses present in a PV system. Its estimation highly depends on the PV modeler skills and experience and directly affects the final energy yield estimation. A probabilistic analysis was performed considering the uncertainty of the derating factors; it was observed that the improper assignment of these factors may lead to rMBE of more than 30% in the estimations of the PV system energy yield. It is also observed that there is not much work devoted to characterize the derating factors present in a PV system, further there is a big spread within the values reported in the literature.

Based on the results of this study, there are suggested future works to assist the designer to make more informed decisions about the losses. Among them, the development of models to replace some of the empirical derating factors that are used in PV modeling today; this would enable a better representation of the effect certain factors have on the PV system energy yield prediction. Perform field measurements in diverse PV system configurations and make them publically available in order to provide better guidance to the modeler for assigning the derates according to the system characteristics.

Acknowledgements

The authors are thankful to the Univ Estadual Paulista (UNESP), Engineering Faculty, Guaratinguetá Campus, for providing the necessary facilities for the preparation of the paper. The research for this paper was financially supported by the Coordination for the Improvement of Higher Education Personnel (CAPES), through the mechanical engineering post-graduation course UNESP/FEG (#33004080027P6). Also, the first author is indebted to People Program (Marie Curie Actions) of the European Union's Seventh Framework Programme FP7/2007–2013/ under project ELECON – Electricity Consumption Analysis to Promote Energy Efficiency Considering Demand Response and Non-technical Losses, REA grant agreement No 318912.

References

[1] Empresa de Pesquisa Energética (EPE). Projeção da demanda de energia elétrica para os próximos 10 anos (2014–2023). Rio de Janeiro; 2013.
[2] Pereira EB, Ramos Martins S, de Abreu Fernando Luna, Ricardo R. Atlas Brasileiro de Energia Solar, 1st ed.. Sao José Dos Campos: SWERA; 2006.
[3] Ribeiro AED, Arouca MC, Coelho DM. Electric energy generation from small-scale solar and wind power in Brazil: the influence of location, area and shape. Renew Energy 2016;85:554–63.
[4] Huld T, Dunlop E, Beyer HG, Gottschalg R. Data sets for energy rating of photovoltaic modules. Sol Energy 2013;93:267–79.
[5] Connolly D, Lund H, Mathiesen BV, Leahy M. A review of computer tools for analysing the integration of renewable energy into various energy systems. Appl Energy 2010;87(4):1059–82.
[6] Richter M, Kalisch J, Schmidt T, Elke L. Best practice guide on uncertainty in PV modelling; 2015.
[7] Yates T, Hibberd B. Production Modeling for Grid-Tied PV,. SolarPRO 2010:30–56.
[8] Lee GR, Frearson L, Rodden P. An assessment of photovoltaic modelling software using real world performance data. In Proceedings of the 26th European photovoltaic solar energy conference and exhibition; 2011. p. 4339–43.
[9] Freeman J, Whitmore, N, Blair, AP. Dobos validation of multiple tools for flat plate photovoltaic modeling against measured data. In: 2014 IEEE Proceedings of the 40th Photovoltaic Specialist Conference (PVSC); 2014, no. August, p. 1932–7.
[10] Cameron CP, Boyson WE, Riley DM. Comparison of PV system performance-model predictions with measured PV system performance. In: Conference Rec. IEEE Photovolt. Spec. Conference; 2008. p. 2–7.
[11] Klise GT, Stein JS. Models used to assess the performance of photovoltaic systems, Albuquerque, 2009; 2009.
[12] Mehleri ED, Zervas PL, Sarimveis H, Palyvos JA, Markatos NC. Determination of the optimal tilt angle and orientation for solar photovoltaic arrays. Renew Energy 2010;35(11):2468–75.
[13] Lave M, Hayes W, Pohl A, Hansen CW. Evaluation of global horizontal irradiance to plane-of-array irradiance models at locations across the United States,. IEEE J Photovolt 2015;5(2):597–606.
[14] Dervishi S, Mahdavi A. Computing diffuse fraction of global horizontal solar radiation: a model comparison. Sol Energy 2012;86(6):1796–802.
[15] Notton G, Cristofari C, Muselli M, Poggi P. Calculation on an hourly basis of solar diffuse irradiations from global data for horizontal surfaces in Ajaccio,. Energy Convers Manag 2004;45(18–19):2849–66.
[16] Orgill JF, Hollands KGT. Correlation equation for hourly diffuse radiation on a horizontal surface. Sol Energy 1977;19(4):357–9.
[17] Iqbal M. An introduction to solar radiation, 1st ed.. Ontario: Academic Press; 1983.
[18] Erbs DG, Klein SA, Duffie JA. Estimation of the Diffuse Radiation Fraction for Hourly, Daily, and Monthly-Average Global Radiation,. Sol Energy 1982;28(4):293.
[19] Maxwell EL. A quasi-physical model for converting hourly global to direct normal insolation, Golden, Colorado; 1987.
[20] Ineichen P, Perez R, Seal RD, Maxwell EL, Zalenka A. Dynamic global-to-direct irradiance conversion models,. ASHRAE Trans 1992;98(1):354–69.
[21] Noorian AM, Moradi I, Kamali GA. Evaluation of 12 models to estimate hourly diffuse irradiation on inclined surfaces. Renew Energy 2008;33:1406–12.
[22] Liu BYH, Jordan RC. The long-term average performance of flat-plate solar energy collectors: with design data for the U.S., its outlying possessions and Canada,. Sol Energy 1963;7(2).
[23] Koronakis PS. On the choice of the angle of tilt for south facing solar collectors in the Athens basin area. Sol Energy 1986;36(3):217–25.
[24] Badescu V. 3D isotropic approximation for solar diffuse irradiance on tilted surfaces. Renew Energy 2002;26(2):221–33.
[25] Tian YQ, Davies-Colley RJ, Gong P, Thorrold BW. Estimating solar radiation on slopes of arbitrary aspect. Agric For Meteor 2001;109:67–74.
[26] Jiménez JI, Castro Y. Solar radiation on sloping surfaces with different orientations in granada, Spain. Sol Energy 1982;28(3):257–62.
[27] Reindl DT, Beckman WA, Duffie JA. Evaluation of hourly tilted surface radiation models. Sol Energy 1990;45(1):9–17.
[28] Duffie JA, Beckman WA. Solar engineering for thermal processes, 4th ed.. New York: Wiley; 2013.
[29] Temps RC, Coulson KL. Solar radiation incident upon slopes of different orientations. Sol Energy 1977;19(1):179–84.
[30] Hay J. Calculation of monthly mean solar radiation for horizontal and tilted surfaces. Sol Energy 1979;23.
[31] Skartveit A, Olseth J Asle. Modelling slope irradiance at high latitudes. Sol Energy 1986;36(4):333–44.
[32] Perez R, Seals R, Ineichen P, Stewart R, Menicucci D. A new simplified version of the perez diffuse irradiance model for tilted surfaces. Sol Energy 1987;39(3):221–31.
[33] Klucher TM. Evaluation of models to predict insolation on tilted surfaces. Sol Energy 1979;23:111–4.
[34] Hay J, Davies JA. Calculation of the solar radiation incident on an inclined surface. In: Proceedings First Canadian Solar Radiation Data Workshop; 1980. p. 59–72.
[35] Perez R, Ineichen P, Seals R, Michalsky J, Stewart R. Modeling daylight availability and irradiance components from direct and global irradiance. Sol Energy 1990;44(5):271–89.
[36] Bugler JW. The determination of hourly insolation on an inclined plane using a diffuse irradiance model based on hourly measured global horizontal insolation. Sol Energy 1977;19:477–91.
[37] Steven MD, Unsworth MH. The angular distribution and interception of diffuse solar radiation below overcast skies. Q J R Meteorol Soc . 1980;106(447):57–61.
[38] Ma CCY, Iqbal M. Statistical comparison of models for estimating solar radiation on inclined surfaces. Sol Energy 1983;31(3):313–7.
[39] Willmott CJ. On the climatic optimization of the tilt and azimuth of flat-plate solar collectors. Sol Energy 1982;28(3):205–16.
[40] Gueymard C. An anisotropic solar irradiance model for tilted surfaces and its comparison with selected engineering algorithms. Sol Energy 1987;38(5):367–86.
[41] Muneer T. Solar radiation and daylight models for the energy efficient design of buildings. Arquit Press 1997;26:197–200.
[42] Yadav AK, Chandel SS. Tilt angle optimization to maximize incident solar radiation: a review. Renew Sustain Energy Rev 2013;23:503–13.
[43] Jakhrani AQ, Samo SR, Rigit ARH, Kamboh SA. Selection of models for calculation of incident solar radiation on tilted surfaces. World Appl Sci J 2013;22(9):1334–43.
[44] Benghanem M. Optimization of tilt angle for solar panel: case study for Madinah, Saudi Arabia. Appl Energy 2011;88(4):1427–33.
[45] Hottel HC, Woertz BB. Performance of flat-plate solar-heat collectors. Trans Am Soc Mech Eng 1942;64:91.
[46] Demain C, Journée M, Bertrand C. Evaluation of different models to estimate the global solar radiation on inclined surfaces. Renew Energy 2013;50:710–21.
[47] Gilman P. SAM photovoltaic model (pvsamv1) technical reference; 2014.
[48] Djamila M, Ernest R. Modeling of solar irradiance and cellsIn: optimization of photovoltaic power systems: modelization, simulation and control. London, UK: Springer-Verlag London Limited; 2012. p. 31–87.
[49] Lambert T, Gilman P, Lilienthal P. Micropower system modeling with HomerIn: Integration of alternative sources of energy. John Wiley & Sons Inc.; 2006. p. 379–418.
[50] Diaf S, Diaf D, Belhamel M, Haddadi M, Louche A. A methodology for optimal sizing of autonomous hybrid PV/wind system. Energy Policy . 2007;35(11):5708–18.
[51] Evans DL. Simplified method for predicting photovoltaic array output. Sol Energy 1981;27(6):555–60.
[52] De Soto W, Klein SA, Beckman WA. Improvement and validation of a model for photovoltaic array performance. Sol Energy 2006;80(1):78–88.
[53] Villalva MG, Gazoli JR, Filho ER. Comprehensive approach to modeling and simulation of photovoltaic arrays. IEEE Trans Power Electron 2009;24(5):1198–208.
[54] Villalva MG, Gazoli JR. Modeling and circuit-based simulation of photovoltaic

arrays. In: Power Electronics Conference 2009; Sep. 2009. p. 1244–54.
[55] Walker G. Evaluating MPPT converter topologies using a MATLAB PV model. J Electr Electron Eng 2001;21(1):49–55.
[56] Gergaud O, Multon B, Ben Ahmed H. Analysis and experimental validation of various photovoltaic system models. In: Proceedings of the 7th International ELECTRIMACS Congress Montréal, no. August; 2002. p. 1–7.
[57] Jones AD, Underwood CP. A modelling method for building-integrated photovoltaic power supply. Build Serv Eng Res Technol 2002;23(3):167–77.
[58] Patel MR. Wind and solar power systems, 1st ed.. Boca Raton: CRC Press; 1999.
[59] Chedid R, Saliba Y. Optimization and control of autonomous renewable energy systems,. Int J Energy Res 1996;20:609–24, [no. October 1994].
[60] Siddiqui MU, Abido M. Parameter estimation for five- and seven-parameter photovoltaic electrical models using evolutionary algorithms. Appl Soft Comput 2013;13(12):4608–21.
[61] D.L. King, W.E. Boyson and J.A. Kratochvill. Photovoltaic Array Performance Model. Report no. SAND2004-3535. pp. 1–43, 2004 [Online]. Available: < http://prod.sandia.gov/techlib/access-control.cgi/2004/043535.pdf > [accessed 10.1.2016]
[62] Marion B, Rummel S, Anderberg A. Current–voltage curve translation by bilinear interpolation. Prog Photovolt Res Appl 2004;12(8):593–607.
[63] Ciulla G, Lo Brano V, Di Dio V, Cipriani G. A comparison of different one-diode models for the representation of I–V characteristic of a PV cell. Renew Sustain Energy Rev 2014;32:684–96.
[64] Wolf M, Rauschenbach H. Series resistance effects on solar cells measurements,. Adv Energy Convers 1963;3(2):455–79.
[65] de Blas MA, Torres JL, Prieto E, García A. Selecting a suitable model for characterizing photovoltaic devices, [Mar.]. Renew Energy 2002;25(3):371–80.
[66] Ma T, Yang H, Lu L. Solar photovoltaic system modeling and performance prediction,. Renew Sustain Energy Rev 2014;36:304–15.
[67] Gow J a, Manning CD. Development of a photovoltaic array model for use in power-electronics simulation studies,. IEE Proc - Electr Power Appl 1999;146(2):193.
[68] Oi A, Anwari M. In: Taufik, modeling and simulation of photovoltaic water pumping system. In: 2009 Proceedings of the third Asia international conference modelling and Simulation; 2009. p. 497–502.
[69] Townsend TU. A method for estimating the long-term performance of direct-coupled photovoltaic systems. Madison: University of Wisconsin; 1989.
[70] Celik AN, Acikgoz N. Modelling and experimental verification of the operating current of mono-crystalline photovoltaic modules using four- and five-parameter models. Appl Energy 2007;84(1):1–15.
[71] Ortiz-Conde A, García Sánchez FJ, Muci J. New method to extract the model parameters of solar cells from the explicit analytic solutions of their illuminated I–V characteristics. Sol Energy Mater Sol Cells 2006;90(3):352–61.
[72] Tamrakar R, Gupta A. A review extraction of solar cell modelling parameters. IJIREEICE 2015;3(1):55–60.
[73] Sellami A, Bouaïcha M. Application of the genetic algorithms for identifying the electrical parameters of PV solar generators. In: Kosyachenko A, editor. Sol. Cells-Silicon Wafer-Based Technol.. InTech; 2011. p. 349–64.
[74] Zagrouba M, Sellami A, Bouaïcha M, Ksouri M. Identification of PV solar cells and modules parameters using the genetic algorithms: application to maximum power extraction. Sol Energy 2010;84(5):860–6.
[75] Saravanan C. A comprehensive analysis for extracting single diode PV model parameters by hybrid GA-PSO algorithm. Int J Comput Appl 2013;78(8):78–81.
[76] Peng W, Zeng Y, Gong H, Leng YQ, Yan YH, Hu W. Evolutionary algorithm and parameters extraction for dye-sensitised solar cells one-diode equivalent circuit model. Micro Nano Lett 2013;8:86–9.
[77] Ishaque K, Salam Z, Mekhilef S, Shamsudin A. Parameter extraction of solar photovoltaic modules using penalty-based differential evolution. Appl Energy 2012;99:297–308, [no. July 2015].
[78] Azab M, Salem F, Mosaad MI. PV parameters estimation using different evolutionary algorithms. J Electr Eng 2014:1–9.
[79] Powell MJD. A new algorithm for unconstrained optimization. Nonlinear Prog. 1970:31–65.
[80] Venkataraman P. Applied optimization with Matlab programming, 2nd ed.. New York: Wiley; 2002.
[81] Skoplaki E, Palyvos JA. On the temperature dependence of photovoltaic module electrical performance: a review of efficiency/power correlations,. Sol Energy 2009;83(5):614–24.
[82] González-longatt FM, Model of Photovoltaic Module in Matlab™. In: 2do Congresso Iberoamericano de Estudiantes de Ingeniería Eléctrica, Electrónica y Computación (CIBELEC); 2005. p. 1–5.
[83] Eckstein JH. Detailed Modelling of phtovoltaic system components. University of Wisconsin; 1990.
[84] Driesse A, Jain P, Harrison S. Beyond the curves: modeling the electrical efficiency of photovoltaic inverters. In: Conference record. IEEE photovoltaic specialists conference; no. August 2008.
[85] Dobos AP. PVWatts version 5 manual (NREL/TP-6A20-62641). Denver; 2014.
[86] Manwell JF, Rogers A, Hayman G, Avelar CT, McGowan JG, Abdulwahid U, Wu K. Hybrid2 - A Hybrid System Simulation Model - Theory Manual, Massachusetts, 2006; 2006.
[87] Notton G, Lazarov V, Stoyanov L. Optimal sizing of a grid-connected PV system for various PV module technologies and inclinations, inverter efficiency characteristics and locations. Renew Energy 2010;35(2):541–54.
[88] Centeno Gonzalez FO, Mahkamov K, Silva Lora EE, Andrade RV, Lesme Jaen R. Prediction by mathematical modeling of the behavior of an internal combustion engine to be fed with gas from biomass, in comparison to the same engine fueled with gasoline or methane. Renew Energy 2013;60:427–32.
[89] King DL, Gonzalez S, Galbraith GM, Boyson WE. Performance model for grid-connected photovoltaic inverters, SAND2007-5036. Contract 2007;38:655–60.
[90] Aprilia EC, Cuk V, Cobben JFG, Ribeiro PF, Kling WL. Modeling the frequency response of photovoltaic inverters. In: IEEE PES Innovative Smart Grid Technologies Conference Europe; 2012. p. 4–8.
[91] Schmid J, von Dincklage RD. European Commission: Euroforum new energies, vol. 3. Invited papers, forum summaries and workshop papers. In Euroforum new energies; 1988. pp. 241–243.
[92] Mondol JD, Yohanis YG, Norton B. Optimal sizing of array and inverter for grid-connected photovoltaic systems. Sol Energy 2006;80(12):1517–39.
[93] Kim N-Y, Ropp M. Study of the initial light-induced degradation of PV modules using N-type dendritic web silicon cells, Conference record. In: 2006 IEEE proceedings of the 4th world conference photovoltaic energy conversion, vol. 2; 2006. 2212–2215.
[94] Mondol JD, Yohanis Y, Smyth M, Norton B. Long term performance analysis of a grid connected photovoltaic system in Northern Ireland. Energy Convers Manag 2006;47(18–19):2925–47.
[95] Notton G, Poggi P, Cristofari C. Predicting hourly solar irradiations on inclined surfaces based on the horizontal measurements: performances of the association of well-known mathematical models. Energy Convers Manag 2006;47:1816–29.
[96] De Miguel A, Bilbao J, Aguiar R, Kambezidis H, Negro E. Diffuse solar irradiation model evaluation in the North Mediterranean Belt area. Sol Energy 2001;70(2):143–53.
[97] Mattei M, Notton G, Cristofari C, Muselli M, Poggi P. Calculation of the polycrystalline PV module temperature using a simple method of energy balance. Renew Energy 2006;31(4):553–67.
[98] Khalil S a, Shaffie aM. Performance of statistical comparison models of solar energy on horizontal and inclined surface. Int J Energy Power 2013;2(1):8–25.
[99] Gueymard CA. Direct and indirect uncertainties in the prediction of tilted irradiance for solar engineering applications. Sol Energy 2009;83(3):432–44.
[100] Notton G, Cristofari C, Poggi P. Performance evaluation of various hourly slope irradiation models using Mediterranean experimental data of Ajaccio. Energy Convers Manag 2006;47(2):147–73.
[101] Jacovides CP, Tymvios FS, Assimakopoulos VD, Kaltsounides NA. Comparative study of various correlations in estimating hourly diffuse fraction of global solar radiation. Renew Energy 2006;31(15):2492–504.
[102] Schnitze M, Thuman C, Johnson P. Reducing uncertainty in solar energy estimates - mitigating energy risk through on-site monitoring; 2012.
[103] Marion B, Adelstein J, Boyle K, Hayden H, Hammond B, Fletcher T, Canada B, Narang D, Shugar D, Wenger H, Kimber A, Mitchell , Rich G, Townsend T. Performance parameters for grid-connected PV Systems. In: Proceedings of the 31st IEEE photovoltaics specialists conference and exhibition; 2005, p. 9.
[104] Stein JS, Cameron CP, Bourne B, Kimber A, Posbic J, Jeste T. A standardized approach to PV system performance model validation. In: Conference Records IEEE Photovoltaic Specialists Conference; 2010. p. 1079–84.
[105] Thevenard D, Pelland S. Estimating the uncertainty in long-term photovoltaic yield predictions,. Sol Energy 2013;91:432–45.
[106] HOMER Energy LLC. Boulder Colorado, 10256 - PV derating factor, *Knowledgebase: Derating Factor*, 2010. [Online]. Available: ⟨http://support.homerenergy.com/index.php?/Knowledgebase/Article/View/183/71/10256—pv-derating-factor-in-homer⟩ [accessed 10.08.15].
[107] Freeman J, Whitmore J, Blair N, Dobos AP. Validation of multiple tools for flat plate photovoltaic modeling against measured data (report); 2014.
[108] Helton JC, Davis FJ. Sampling-based methods for uncertainty and sensitivity analysis (SAND99-2240), Sandia National Laboratories. Albuquerque, USA; 2000.
[109] Buemi D. PV system derates explained, The PV advocate. Available at: ⟨http://davebuemi.com/2011/03/21/pv-system-derates-explained/⟩; 2011.
[110] Pingel S, Koshnicharov D, Frank O, Geipel T, Zemen Y, Striner B, Berghold J. Initial degradation of industrial silicon solar cells in solar panels. In: Proceedings of the 25th European Photovoltaic solar energy conference and exhibition; 2010.
[111] Vartiainen E. A new approach to estimating the diffuse irradiance on inclined surfaces. Renew Energy 2000;20(1):45–64.
[112] Muneer T. Solar radiation modelling for the United Kingdom. CNNA; 1987.
[113] Padovan A, Del Col D. Measurement and modeling of solar irradiance components on horizontal and tilted planes. Sol Energy 2010;84(12):2068–84.
[114] Perez R, Stewart R, Arbogast C, Seals R, Scott J. An anisotropic hourly diffuse radiation model for sloping surfaces: description, performance validation, site dependency evaluation. Sol Energy 1986;36(6):481–97.
[115] Freeman J, Whitmore J, Kaffine L, Blair N, Dobos AP. System advisor model: flat plate photovoltaic performance modeling validation report. Golden, Colorado; 2013.
[116] Mondol JD, Yohanis YG, Norton B. Comparison of measured and predicted long term performance of grid a connected photovoltaic system. Energy Convers Manag 2007;48(4):1065–80.
[117] Sinha S, Chandel SS. Review of software tools for hybrid renewable energy systems. Renew Sustain Energy Rev 2014;32:192–205.